

Bayesian Optimization-based Combinatorial Assignment[†]

Jakob Weissteiner,^{*1,3} Jakob Heiss,^{*2,3} Julien Siems,^{*1} Sven Seuken^{1,3}

¹University of Zurich

²ETH Zurich

³ETH AI Center

weissteiner@ifi.uzh.ch, jakob.heiss@math.ethz.ch, juliensiems@gmail.com, seuken@ifi.uzh.ch

Abstract

We study the combinatorial assignment domain, which includes combinatorial auctions and course allocation. The main challenge in this domain is that the bundle space grows exponentially in the number of items. To address this, several papers have recently proposed *machine learning-based preference elicitation* algorithms that aim to elicit only the most important information from agents. However, the main shortcoming of this prior work is that it does not model a mechanism’s uncertainty over values for not yet elicited bundles. In this paper, we address this shortcoming by presenting a *Bayesian Optimization-based Combinatorial Assignment (BOCA)* mechanism. Our key technical contribution is to integrate a method for capturing model uncertainty into an iterative combinatorial auction mechanism. Concretely, we design a new method for estimating an *upper uncertainty bound* that can be used to define an acquisition function to determine the next query to the agents. This enables the mechanism to properly *explore* (and not just *exploit*) the bundle space during its preference elicitation phase. We run computational experiments in several spectrum auction domains to evaluate BOCA’s performance. Our results show that BOCA achieves higher allocative efficiency than state-of-the-art approaches.

1 Introduction

Many economic problems require finding an efficient combinatorial assignment of multiple indivisible items to multiple agents. Popular examples include *combinatorial auctions (CAs)*, *combinatorial exchanges (CEs)*, and *combinatorial course allocation*. In CAs, heterogeneous items are allocated among a set of bidders, e.g., for the sale of spectrum licenses (Cramton 2013). In CEs, items are allocated among agents who can be sellers *and* buyers at the same time, e.g., for the reallocation of catch shares (Bichler, Fux, and Goeree 2019). In course allocation, course seats are allocated among students at universities (Budish 2011).

In all these domains, agents have preferences over *bundles* of items. In particular, agents’ preferences may exhibit *complementarities* and *substitutabilities* among items. A mechanism that allows agents to report values for bundles rather than just for individual items can achieve significantly

higher efficiency. However, this also implies that agents’ preferences are exponentially-sized (i.e., for m items there are 2^m different bundles), which implies that agents cannot report values for all bundles. Therefore, the key challenge in combinatorial assignment is the design of a *preference elicitation (PE)* algorithm that is (i) *practically feasible* w.r.t. elicitation costs and (ii) *smart*, i.e., it should elicit the information that is “most useful” for achieving high efficiency.

1.1 Iterative Combinatorial Auctions (ICAs)

While the PE challenge is common to all combinatorial assignment problems, it has been studied most intensely in the CA domain (Sandholm and Boutilier 2006). In CAs with general valuations, the amount of communication needed to guarantee full efficiency is exponential in the number of items (Nisan and Segal 2006). Thus, practical CAs cannot provide efficiency guarantees. In practice, *iterative combinatorial auctions (ICAs)* are therefore employed, where the auctioneer interacts with bidders over rounds, eliciting a *limited* (and thus *practically feasible*) amount of information, aiming to find a highly efficient allocation. ICAs are widely used; e.g., for the sale of licenses to build offshore wind farms (Ausubel and Cramton 2011). The provision of spectrum licenses via the *combinatorial clock auction (CCA)* (Ausubel, Cramton, and Milgrom 2006) has generated more than \$20 billion in total revenue (Ausubel and Baranov 2017). Thus, increasing the efficiency of such real-world ICAs by only 1% point translates into monetary gains of hundreds of millions of dollars.

1.2 ML-powered Preference Elicitation

In recent years, researchers have used machine learning (ML) to design smart PE algorithms. Most related to this paper is the work by Brero, Lubin, and Seuken (2018, 2021), who developed the first practical ML-powered ICA that outperforms the CCA. The main idea of their mechanism is two-fold: first, they train a separate *support vector regression* model to learn each bidder’s full value function from a small set of bids; second, they solve an *ML-based winner determination problem (WDP)* to determine the allocation with the highest predicted social welfare, and they use this allocation to generate the next set of queries to all bidders. This process repeats in an iterative fashion until a fixed number of queries has been asked. Thus, their ML-powered ICA

^{*}These authors contributed equally.

[†]This paper is the full version of Weissteiner et al. (2023) published at AAI’23 including the appendix.

can be interpreted as a form of combinatorial *Bayesian Optimization* (BO) (see Appendix C; also see Section 2.3 for a review of BO).

In several follow-up papers, this work has been extended by developing more sophisticated ML methods for this problem. Weissteiner and Seuken (2020) integrated *neural networks* (NN) in their ICA and further increased efficiency. Weissteiner et al. (2022b) used *Fourier transforms* (FTs) to leverage different notions of sparsity of value functions. Finally, Weissteiner et al. (2022a) achieved state-of-the-art (SOTA) performance using *Monotone-Value NNs* (MVNNs), which incorporate important prior domain knowledge.

The main shortcoming of this prior work is that all of these approaches are *myopic* in the sense that the resulting mechanisms simply query the allocation with the highest predicted welfare. In particular, the mechanisms do not have any model of *uncertainty* over bidders’ values for not yet elicited bundles, although handling uncertainty in a principled manner is one of the key requirements of a smart PE algorithm (Bonilla, Guo, and Sanner 2010). Thus, the mechanisms cannot properly control the *exploration-exploitation trade-off* inherent to BO. For ML-based ICAs, this means that the mechanisms may get stuck in local minima, repeatedly querying one part of the allocation space while not exploring other, potentially more efficient allocations.

1.3 Our Contributions

In this paper, we address this main shortcoming of prior work and show how to integrate a notion of *model uncertainty* (i.e., epistemic uncertainty) over agents’ preferences into iterative combinatorial assignment. Concretely, we design a *Bayesian Optimization-based combinatorial assignment* (BOCA)¹ mechanism that makes use of model uncertainty in its query generation module. The main technical challenge is to design a new method for estimating an *upper uncertainty bound* that can be used to define an acquisition function to determine the next query. To this end, we combine MVNNs (Weissteiner et al. 2022a) with *Neural optimization-based Model Uncertainty* (NOMU) (Heiss et al. 2022), a recently introduced method to estimate model uncertainty for NNs. In detail, we make the following contributions:

1. We present a modified NOMU algorithm (Section 3.1), tailored to CAs, exploiting monotonicity of agents’ preferences and the discrete (finite) nature of this setting.
2. We show that generic parameter initialization for monotone NNs can dramatically fail and propose a new initialization method for MVNNs based on uniform mixture distributions (Section 3.2).
3. We present a more succinct mixed integer linear program for MVNNs to solve the ML-based WDP (Section 3.3).
4. We experimentally show that BOCA outperforms prior approaches in terms of efficiency (Section 4).

Although our contribution applies to any combinatorial assignment setting, we focus on CAs to simplify the notation

¹The acronym BOCA has also been used for a different method, namely for *Bayesian Optimisation with Continuous Approximations* by Kandasamy et al. (2017).

and because there exist well-studied preference generators for CAs that we use for our experiments.

Our source code is available on GitHub: <https://github.com/marketdesignresearch/BOCA>.

1.4 Related Work on Model Uncertainty

Estimating model uncertainty for NNs is an active area of research in AI and ML, with a plethora of new methods proposed every year. Classic methods can be broadly categorized into (i) *ensemble methods*: training multiple different NNs to estimate model uncertainty (Gal and Ghahramani 2016; Lakshminarayanan, Pritzel, and Blundell 2017; Wenzel et al. 2020) and (ii) *Bayesian NNs* (BNNs): assuming a prior distribution over parameters and then estimating model uncertainty by approximating the intractable posterior (Graves 2011; Blundell et al. 2015; Hernández-Lobato and Adams 2015; Ober and Rasmussen 2019). However, for ML-based iterative combinatorial assignment, a key requirement is to be able to efficiently solve the ML-based WDP based on these uncertainty estimates. As there is no known computationally tractable method to perform combinatorial optimization over ensembles or BNNs, we cannot use these approaches for ML-based ICAs. In contrast, NOMU (Heiss et al. 2022) enables the computationally efficient optimization over its uncertainty predictions, which is why we use it as a building block for BOCA.

2 Preliminaries

In this section, we present our formal model (Section 2.1), review the ML-based ICA by Brero, Lubin, and Seuken (2021) (Section 2.2), briefly review Bayesian optimization (BO) (Section 2.3), and review *monotone-value neural networks* (MVNNs) by Weissteiner et al. (2022a) (Section 2.4) as well as *neural optimization-based model uncertainty* (NOMU) by Heiss et al. (2022) (Section 2.5).

2.1 Formal Model for ICAs

We consider a CA with n bidders and m indivisible items. Let $N = \{1, \dots, n\}$ and $M = \{1, \dots, m\}$ denote the set of bidders and items. We denote by $x \in \mathcal{X} = \{0, 1\}^m$ a bundle of items represented as an indicator vector, where $x_j = 1$ iff item $j \in M$ is contained in x . Bidders’ true preferences over bundles are represented by their (private) value functions $v_i : \mathcal{X} \rightarrow \mathbb{R}_+$, $i \in N$, i.e., $v_i(x)$ represents bidder i ’s true value for bundle $x \in \mathcal{X}$.

By $a = (a_1, \dots, a_n) \in \mathcal{X}^n$ we denote an allocation of bundles to bidders, where a_i is the bundle bidder i obtains. We denote the set of *feasible* allocations by $\mathcal{F} = \{a \in \mathcal{X}^n : \sum_{i \in N} a_{ij} \leq 1, \forall j \in M\}$. We let $p \in \mathbb{R}_+^n$ denote the bidders’ payments. We assume that bidders have quasilinear utility functions u_i of the form $u_i(a, p) = v_i(a_i) - p_i$. This implies that the (true) *social welfare* $V(a)$ of an allocation a is equal to the sum of all bidders’ values $\sum_{i \in N} v_i(a_i)$. We let $a^* \in \operatorname{argmax}_{a \in \mathcal{F}} V(a)$ denote a social-welfare maximizing, i.e., *efficient*, allocation. The *efficiency* of any allocation $a \in \mathcal{F}$ is determined as $V(a)/V(a^*)$.

An ICA *mechanism* defines how the bidders interact with the auctioneer and how the allocation and payments are determined. We denote a bidder’s (possibly untruthful) reported value function by $\hat{v}_i : \mathcal{X} \rightarrow \mathbb{R}_+$. In this paper, we consider ICAs that ask bidders to iteratively report their values $\hat{v}_i(x)$ for bundles x selected by the mechanism. A finite set of reported bundle-value pairs of bidder i is denoted as $R_i = \{(x^{(l)}, \hat{v}_i(x^{(l)}))\}$, $x^{(l)} \in \mathcal{X}$. Let $R = (R_1, \dots, R_n)$ be the tuple of reported bundle-value pairs obtained from all bidders. We define the *reported social welfare* of an allocation a given R as $\hat{V}(a|R) := \sum_{i \in N: (a_i, \hat{v}_i(a_i)) \in R_i} \hat{v}_i(a_i)$, where $(a_i, \hat{v}_i(a_i)) \in R_i$ ensures that only values for reported bundles contribute. The ICA’s optimal allocation $a_R^* \in \mathcal{F}$ and payments $p(R) \in \mathbb{R}_+^n$ are computed based on the elicited reports R only. More formally, $a_R^* \in \mathcal{F}$ given reports R is defined as

$$a_R^* \in \operatorname{argmax}_{a \in \mathcal{F}} \hat{V}(a|R). \quad (1)$$

As the auctioneer can only query a limited number of bundles $|R_i| \leq Q^{\max}$ (e.g., $Q^{\max} = 100$), an ICA needs a practically feasible and smart PE algorithm.

2.2 A Machine Learning-powered ICA

We now provide a high-level review of the *machine learning-powered combinatorial auction (MLCA)* by [Brero, Lubin, and Seuken \(2021\)](#) (please see Appendix A for further details). MLCA proceeds in rounds until a maximum number of value queries per bidder Q^{\max} is reached. In each round, for every bidder i , an ML model \mathcal{A}_i is trained on the bidder’s reports R_i to learn an approximation of bidders’ value functions. Next, MLCA generates new value queries by computing the allocation with the highest predicted social welfare. Concretely, it computes $q^{\text{new}} = (q_i^{\text{new}})_{i=1}^n$ with $q_i^{\text{new}} \in \mathcal{X} \setminus R_i$ by solving an ML-based WDP:

$$q^{\text{new}} \in \operatorname{argmax}_{a \in \mathcal{F}} \sum_{i \in N} \mathcal{A}_i(a_i) \quad (2)$$

The idea is the following: if the \mathcal{A}_i ’s are good surrogate models of the bidders’ value functions, then the efficiency of q^{new} is likely to be high as well. Thus, in each round, bidders are providing value reports on bundles that are guaranteed to fit into a feasible allocation and that together are predicted to have high social welfare. Additionally, bidders are also allowed to submit “push-bids,” enabling them to submit information to the auctioneer that they deem useful, even if they are not explicitly queried about it. At the end of each round, MLCA receives reports R^{new} from all bidders for the newly generated queries q^{new} , and updates the overall elicited reports R . When Q^{\max} is reached, MLCA computes an allocation a_R^* that maximizes the *reported* social welfare (Equation (1)) and determines VCG payments $p(R)$ based on all reports (see Appendix Definition B.1).

Remark 1 (IR, No-Deficit, and Incentives of MLCA). [Brero, Lubin, and Seuken \(2021\)](#) showed that MLCA satisfies individual rationality (IR) and no-deficit, with any ML algorithm. They also studied MLCA’s incentive properties; this is important, since manipulations may lower efficiency.

Like all deployed ICAs (including the CCA), MLCA is not strategyproof. However, they argued that it has good incentives in practice; and given two additional assumptions, bidding truthfully is an ex-post Nash equilibrium. We present a detailed summary of their incentive analysis in Appendix B.

2.3 Bayesian Optimization Background

In this section, we briefly review Bayesian optimization (BO). BO refers to a class of *machine learning-based gradient-free* optimization methods, which, for a given black-box objective function $f : X \rightarrow Y$, aim to solve

$$\max_{x \in X} f(x) \quad (3)$$

in an *iterative* manner. Specifically, given a budget of T queries (i.e., function evaluations of f), a BO algorithm generates queries $\{x^{(1)}, \dots, x^{(T)}\}$ with the aim that

$$\max_{x \in \{x^{(1)}, \dots, x^{(T)}\}} f(x) \approx \max_{x \in X} f(x). \quad (4)$$

In each BO step t , the algorithm selects a new input point $x^{(t)} \in X$ and observes a (potentially noisy) output

$$y^{(t)} = f(x^{(t)}) + \varepsilon^{(t)}, \quad (5)$$

where $\varepsilon^{(t)}$ is typically assumed to be i.i.d. Gaussian distributed, i.e., $\varepsilon^{(t)} \sim \mathcal{N}(0, \sigma^2)$.² The BO algorithm’s decision rule for selecting the query $x^{(t)}$ is based on

1. A *probabilistic model* representing an (approximate) posterior distribution over f (e.g., Gaussian processes, NOMU, ensembles, BNNs, etc.).
2. An *acquisition function* $\mathcal{A} : X \rightarrow Y$ that uses this probabilistic model to determine the next query $x^{(t)} \in \operatorname{argmax}_{x \in X} \mathcal{A}(x)$ by properly trading off *exploration* and *exploitation*. Popular examples of acquisition functions include:

- *Upper uncertainty bound* (aka *upper confidence bound (UCB)*) ([Srinivas et al. 2012](#))
- *Expected improvement* ([Frazier 2018](#), Section 4.1)
- *Thompson sampling* ([Chapelle and Li 2011](#))

Remark 2. MLCA (Section 2.2) can be seen as a combinatorial BO algorithm with acquisition function $\mathcal{A} := \sum_{i \in N} \mathcal{A}_i$ (see Appendix C for a discussion).

2.4 MVNNs: Monotone-Value Neural Networks

MVNNs ([Weissteiner et al. 2022a](#)) are a new class of NNs specifically designed to represent *monotone combinatorial* valuations. First, we reprint the definition of MVNNs and then discuss their desirable properties.

Definition 1 (MVNN, [Weissteiner et al. \(2022a\)](#)). An MVNN $\mathcal{M}_i^{\theta} : \mathcal{X} \rightarrow \mathbb{R}_+$ for bidder $i \in N$ is defined as

$$\mathcal{M}_i^{\theta}(x) := W^{i, K_i} \varphi_{0, t^i, K_i - 1}(\dots \varphi_{0, t^i, 1}(W^{i, 1} x + b^{i, 1}) \dots) \quad (6)$$

- $K_i + 1 \in \mathbb{N}$ is the number of layers ($K_i - 1$ hidden layers),

²In this paper, we assume that $\sigma^2 = 0$.

- $\{\varphi_{0,t^{i,k}}\}_{k=1}^{K_i-1}$ are the MVNN-specific activation functions with cutoff $t^{i,k} > 0$, called bounded ReLU (bReLU):

$$\varphi_{0,t^{i,k}}(\cdot) := \min(t^{i,k}, \max(0, \cdot)) \quad (7)$$

- $W^i := (W^{i,k})_{k=1}^{K_i}$ with $W^{i,k} \geq 0$ and $b^i := (b^{i,k})_{k=1}^{K_i-1}$ with $b^{i,k} \leq 0$ are the non-negative weights and non-positive biases of dimensions $d^{i,k} \times d^{i,k-1}$ and $d^{i,k}$, whose parameters are stored in $\theta = (W^i, b^i)$.

MVNNs are particularly well suited for the design of combinatorial assignment mechanism for two reasons. First, MVNNs are *universal* in the set of monotone and normalized value functions (Weissteiner et al. 2022a, Theorem 1), i.e., any $\hat{v}_i : \mathcal{X} \rightarrow \mathbb{R}_+$ that satisfies the following two properties can be represented *exactly* as an MVNN \mathcal{M}_i^θ :

1. **Monotonicity (M)** (“additional items increase value”):
For $A, B \in 2^M$: if $A \subseteq B$ it holds that $\hat{v}_i(A) \leq \hat{v}_i(B)$
2. **Normalization (N)** (“no value for empty bundle”):
 $\hat{v}_i(\emptyset) = \hat{v}_i((0, \dots, 0)) := 0$,

Second, Weissteiner et al. (2022a) showed that an MVNN-based WDP, i.e., $\operatorname{argmax}_{a \in \mathcal{F}} \sum_{i \in N} \mathcal{M}_i^\theta(a_i)$, can be succinctly encoded as a MILP, which is key for the design of MVNN-based iterative combinatorial assignment mechanisms. Finally, Weissteiner et al. (2022a) experimentally showed that using MVNNs as \mathcal{A}_i in MLCA leads to SOTA performance.

2.5 NOMU

Recently, Heiss et al. (2022) introduced a novel method to estimate model uncertainty for NNs: *Neural optimization-based model uncertainty (NOMU)*. In contrast to other methods (e.g., ensembles), NOMU represents an *upper uncertainty bound (uUB)* as a *single* and *MILP-formalizable* NN. Thus, NOMU is particularly well suited for iterative combinatorial assignment, where uUB-based *winner determination problems (WDPs)* need to be solved hundreds of times to generate new informative queries. This, together with NOMU’s strong performance in noiseless BO, is the reason why we build on it and define a modified NOMU algorithm tailored to iterative combinatorial assignment (Section 3.1).

3 Bayesian Optimization-based ICA

In this section, we describe the design of our Bayesian optimization-based combinatorial assignment (BOCA) mechanism. While the design is general, we here present it for the CA setting, leading to a BO-based ICA. Recall that MLCA generates new value queries by solving the ML-based WDP $q^{\text{new}} \in \operatorname{argmax}_{a \in \mathcal{F}} \sum_{i \in N} \mathcal{A}_i(a_i)$ (see Section 2.2).

For the design of BOCA, we integrate a proper notion of uncertainty into MLCA by using a bidder-specific *upper uncertainty bound (uUB)*, taking the role of the ML model \mathcal{A}_i , to define our acquisition function $\mathcal{A} := \sum_{i \in N} \mathcal{A}_i$. To define our uUB and make it amenable to MLCA, we proceed in three steps: First, we combine MVNNs with a modified NOMU algorithm that is tailored to the characteristics of combinatorial assignment (Section 3.1). Second, we highlight the importance of proper parameter

initialization for MVNNs and propose a more robust method (Section 3.2). Third, we present a more succinct MILP for MVNNs (Section 3.3). In the remainder of the paper, we make the following assumption:

Assumption 1. For all agents $i \in N$, the true and reported value functions v_i and \hat{v}_i fulfill the **Monotonicity (M)** and **Normalization (N)** property (see Section 2.4).

3.1 Model Uncertainty for Monotone NNs

We propose a modified NOMU architecture and loss that is specifically tailored to combinatorial assignment. Concretely, our algorithm is based on the following two key characteristics of combinatorial assignment: (i) since agents’ value functions are monotonically increasing, the uUBs need to be monotonically increasing too, and (ii) due to the (finite) discrete input space, one can derive a closed-form expression of the 100%-uUB as an MVNN. Before we present our modified NOMU architecture and loss, we introduce the MVNN-based 100%-uUB.

Let \mathcal{H} denote a *hypothesis class* of functions $f : X \rightarrow Y$ for some input and output spaces X and Y and let $\mathcal{H}_{D^{\text{train}}} := \{f \in \mathcal{H} : f(x^{(l)}) = y^{(l)}, l = 1, \dots, n^{\text{train}}\}$ denote the set of all functions from \mathcal{H} that fit exactly through training points $D^{\text{train}} = \{(x^{(l)}, f(x^{(l)}))\}_{l=1}^{n^{\text{train}}}$.

Definition 2 (100%-uUB). For a hypothesis class \mathcal{H} and a training set D^{train} , we define the 100%-uUB as $f^{100\text{-uUB}}(x) := \sup_{f \in \mathcal{H}_{D^{\text{train}}}} f(x)$ for every $x \in X$.

In the following, let

$$\mathcal{V} := \{\hat{v} : \mathcal{X} \rightarrow \mathbb{R}_+ \mid \text{satisfy (N) and (M)}\} \quad (8)$$

denote the set of all value functions that satisfy the *normalization* and *monotonicity* property. Next, we define the 100%-uUB. In Theorem 1, we show that for $\mathcal{H} = \mathcal{V}$ the 100%-uUB can be explicitly represented as an MVNN.

Theorem 1 (MVNN-based 100%-uUB). Let $((1, \dots, 1), \hat{v}_i(1, \dots, 1)) \in D^{\text{train}}$. Then for $\mathcal{H} = \mathcal{V}$ it holds that $f^{100\text{-uUB}}(x) = \max_{f \in \mathcal{V}_{D^{\text{train}}}} f(x)$ for all $x \in \mathcal{X}$ and $f^{100\text{-uUB}} \in \mathcal{V}_{D^{\text{train}}}$ can be represented as a two hidden layer MVNN with n^{train} neurons per layer, which we denote as $\mathcal{M}_i^{100\text{-uUB}}$ going forward.³

Proof. The proof for Theorem 1 is provided in Appendix D.1. It follows a similar idea as the universality proof in (Weissteiner et al. 2022a, Theorem 1). In particular, Equation (26) in Appendix D.1 provides the closed-form expression of $f^{100\text{-uUB}}$ as MVNN $\mathcal{M}_i^{100\text{-uUB}}$. \square

Using the MVNN-based 100%-uUB $\mathcal{M}_i^{100\text{-uUB}}$, we can now define our modified NOMU architecture and loss.

The Architecture. Towards defining the architecture, we first observe that if the true function is monotonically increasing, the corresponding uUB needs to be monotonically increasing as well (Propositions 1 and 2 in Appendix D.2).

³Note that $\mathcal{M}_i^{100\text{-uUB}}(\cdot)$ depends on a training set D^{train} , but we omit this dependency in our notation to improve readability.

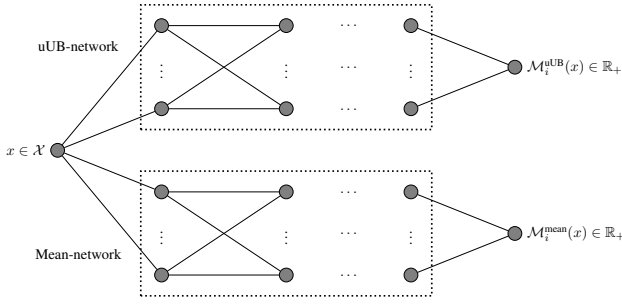


Figure 1: $\mathcal{M}_i^{\text{NOMU}}$: a modification of NOMU’s original architecture for the combinatorial assignment domain

Given that bidders’ value functions are monotone (Assumption 1), this implies that our uUB must also be monotonically increasing. Thus, instead of the original NOMU architecture that outputs the (raw) uncertainty (i.e., an estimate of the posterior standard deviation) which is *not* monotone, we can modify NOMU’s architecture and directly output the monotone uUB. Given this, we propose the following architecture $\mathcal{M}_i^{\text{NOMU}}$ to estimate the uUB for bidder $i \in N$. $\mathcal{M}_i^{\text{NOMU}}$ consists of two sub-MVNNs with two outputs: the mean prediction $\mathcal{M}_i^{\text{mean}} : \mathcal{X} \rightarrow \mathbb{R}$ and the estimated uUB $\mathcal{M}_i^{\text{uUB}} : \mathcal{X} \rightarrow \mathbb{R}$. In Figure 1, we provide a schematic representation of $\mathcal{M}_i^{\text{NOMU}}$ (see Appendix D.2 for details).

The Loss. Next, we formulate a new NOMU loss function L^π tailored to combinatorial assignment. Since we have a closed-form expression of the 100%-uUB as MVNN $\mathcal{M}_i^{100\%-\text{uUB}}$ (Theorem 1), we are able to enforce that $\mathcal{M}_i^{\text{mean}} \leq \mathcal{M}_i^{\text{uUB}} \leq \mathcal{M}_i^{100\%-\text{uUB}}$ via the design of our new loss function. Let $\mathcal{M}_i^{\text{mean}}$ be a trained mean-MVNN with a standard loss (e.g. MAE and L2-regularization). Using $\mathcal{M}_i^{\text{mean}}$ and $\mathcal{M}_i^{100\%-\text{uUB}}$, we then only train the parameters θ of $\mathcal{M}_i^{\text{uUB}}$ with loss L^π and L2-regularization parameter $\lambda > 0$, i.e., minimizing $L^\pi(\mathcal{M}_i^{\text{uUB}}) + \lambda \|\theta\|_2^2$ via gradient descent. In particular, the parameters of $\mathcal{M}_i^{100\%-\text{uUB}}$ and $\mathcal{M}_i^{\text{mean}}$ are not influenced by the training of $\mathcal{M}_i^{\text{uUB}}$ (see Appendix D.3 for details on the loss and training procedure).

Definition 3 (NOMU Loss Tailored to Combinatorial Assignment). Let $\pi = (\pi_{\text{sqr}}, \pi_{\text{exp}}, c_{\text{exp}}, \bar{\pi}, \underline{\pi}) \in \mathbb{R}_+^5$ be a tuple of hyperparameters. For a training set D^{train} , L^π is defined as

$$L^\pi(\mathcal{M}_i^{\text{uUB}}) := \pi_{\text{sqr}} \sum_{l=1}^{n_{\text{train}}} L_1^\beta(\mathcal{M}_i^{\text{uUB}}(x^{(l)}), y^{(l)}) \quad (9a)$$

$$+ \pi_{\text{exp}} \int_{[0,1]^m} g(-c_{\text{exp}}(\min\{\mathcal{M}_i^{\text{uUB}}(x), \mathcal{M}_i^{100\%-\text{uUB}}(x)\} - \mathcal{M}_i^{\text{mean}}(x))) dx \quad (9b)$$

$$+ \pi_{\text{exp}} c_{\text{exp}} \bar{\pi} \int_{[0,1]^m} L_1^\beta((\mathcal{M}_i^{\text{uUB}}(x) - \mathcal{M}_i^{100\%-\text{uUB}}(x))^+) dx \quad (9c)$$

$$+ \pi_{\text{exp}} c_{\text{exp}} \underline{\pi} \int_{[0,1]^m} L_1^\beta((\mathcal{M}_i^{\text{mean}}(x) - \mathcal{M}_i^{\text{uUB}}(x))^+) dx, \quad (9d)$$

where L_1^β is the smooth L1-loss with threshold β (see Appendix Definition D.1), $(\cdot)^+$ the positive part, and $g :=$

$1 + \text{ELU}^4$ is convex monotonically increasing with ELU being the exponential linear unit (ELU) (see Appendix Definition D.2).

The interpretations of the four terms are as follows:

(9a) enforces that $\mathcal{M}_i^{\text{uUB}}$ fits through the training data.

(9b) pushes $\mathcal{M}_i^{\text{uUB}}$ up as long as it is below the 100%-uUB $\mathcal{M}_i^{100\%-\text{uUB}}$. This force gets weaker the further $\mathcal{M}_i^{\text{uUB}}$ is above the mean $\mathcal{M}_i^{\text{mean}}$ (especially if c_{exp} is large). π_{exp} controls the overall strength of (9b) and c_{exp} controls how fast this force increases when $\mathcal{M}_i^{\text{uUB}} \rightarrow \mathcal{M}_i^{\text{mean}}$. Thus, increasing π_{exp} increases the uUB and increasing c_{exp} increases the uUBs in regions where it is close to $\mathcal{M}_i^{\text{mean}}$. Weakening (9b) (i.e., $\pi_{\text{exp}} c_{\text{exp}} \rightarrow 0$) leads to $\mathcal{M}_i^{\text{uUB}} \approx \mathcal{M}_i^{\text{mean}}$. Strengthening (9b) by increasing $\pi_{\text{exp}} c_{\text{exp}}$ in relation to regularization⁵ leads to $\mathcal{M}_i^{\text{uUB}} \approx \mathcal{M}_i^{100\%-\text{uUB}}$.

(9c) enforces that $\mathcal{M}_i^{\text{uUB}} \leq \mathcal{M}_i^{100\%-\text{uUB}}$. The strength of this term is determined by $\bar{\pi} \cdot (\pi_{\text{exp}} c_{\text{exp}})$, where $\bar{\pi}$ is the (9c)-specific hyperparameter and $\pi_{\text{exp}} c_{\text{exp}}$ adjusts the strength of (9c) to (9b).

(9d) enforces $\mathcal{M}_i^{\text{uUB}} \geq \mathcal{M}_i^{\text{mean}}$. The interpretation of $\underline{\pi}$ and $\pi_{\text{exp}} c_{\text{exp}}$ is analogous to (9c).

As in (Heiss et al. 2022), in the implementation of L^π , we approximate Equations (9b) to (9d) via Monte Carlo integration using additional, *artificial input points* $D^{\text{art}} := \{x^{(l)}\}_{l=1}^{n_{\text{art}}} \stackrel{i.i.d.}{\sim} \text{Unif}([0, 1]^m)$.

Visualization of the uUB. In Figure 2, we present a visualization of the output of $\mathcal{M}_i^{\text{NOMU}}$ (i.e., $\mathcal{M}_i^{\text{mean}}$ and $\mathcal{M}_i^{\text{uUB}}$) and $\mathcal{M}_i^{100\%-\text{uUB}}$ for the national bidder in the LSVM domain of the spectrum auction test suite (SATS) (Weiss, Lubin, and Seuken 2017). In noiseless regression, uncertainty should vanish at observed training points, but (model) uncertainty should remain about value predictions for bundles that are very different from the bundles observed in training. Figure 2 shows that our uUB $\mathcal{M}_i^{\text{uUB}}$ nicely fulfills this. Moreover, we have shown in Appendix D.2 that $\mathcal{M}_i^{\text{uUB}}$ is monotonically increasing, since we assume that value functions fulfill the monotonicity property. This implies that once we observe a value for the full bundle, we obtain a globally bounded 100%-uUB, i.e., see $\mathcal{M}_i^{100\%-\text{uUB}}$ in Figure 2. Furthermore, we see that $\mathcal{M}_i^{100\%-\text{uUB}}$ jumps to a high value when only a single item is added to an already queried bundle, but then often stays constant (e.g., $|x| = 12, \dots, 18$ in Figure 2). Thus, using such a 100%-uUB in our acquisition function, BOCA would only add a single item to an already queried bundle to have more items left for the other bidders instead of properly exploring the bundle space. Our uUB $\mathcal{M}_i^{\text{uUB}}$ circumvents this via implicit and explicit regularization and yields a useful uUB.

3.2 Parameter Initialization for MVNNs

We now discuss how to properly initialize parameters for MVNNs. Importantly, the *MVNN-based uUBs* $\mathcal{M}_i^{\text{uUB}}$ are

⁴In our notation, $g(\cdot)$ is the analog of the function $e^{(\cdot)}$ used in the original NOMU loss in (Heiss et al. 2022).

⁵Regularization can be early stopping or a small number of neurons (implicit) or L2-regularization on the parameters (explicit).

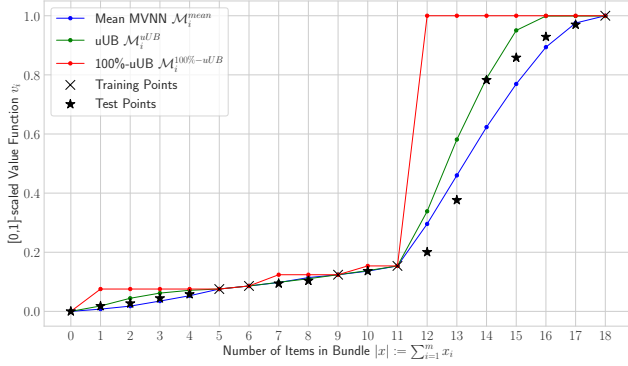


Figure 2: $\mathcal{M}_i^{\text{mean}}$, $\mathcal{M}_i^{\text{uUB}}$ and $\mathcal{M}_i^{\text{100%-uUB}}$ along an increasing 1D subset-path (i.e., for all bundles $x^{(j)}, x^{(k)}$ on the x-axis it holds that for $j \leq k : x^{(j)} \subset x^{(k)}$).

MVNNs. As we will show next, to achieve the best performance of BOCA (in fact of any MVNN training), an adjusted, non-generic parameter initialization is very important.

Generic Initialization. For standard NNs, it is most common to use a weight initialization with zero mean $\mu_k := \mathbb{E} [W_{j,l}^{i,k}] = 0$ and non-zero variance $\sigma_k^2 := \mathbb{V} [W_{j,l}^{i,k}] \neq 0$. Then the mean of each pre-activated neuron of the first hidden layer is zero and the variance $\mathbb{V} [(W^{i,1}x)_j] = d^{i,0} \sigma_1^2 \bar{x}^2$, if $(W_{j,l}^{i,1})_{l=1}^{d^{i,0}}$ are i.i.d., where $\bar{x}^2 = \frac{1}{d^{i,0}} \sum_{l=1}^{d^{i,0}} x_l^2$.⁶ Analogously, one can compute the *conditional* mean and the *conditional* variance of a pre-activated neuron in any layer k by replacing x by the output $z^{i,k-1}$ of the previous layer, i.e., $\mathbb{E} [(W^{i,k} z^{i,k-1})_j | z^{i,k-1}] = 0$ and $\mathbb{V} [(W^{i,k} z^{i,k-1})_j | z^{i,k-1}] = d^{i,k-1} \sigma_k^2 (z^{i,k-1})^2$. For $\sigma_k \propto \frac{1}{\sqrt{d^{i,k-1}}}$, the conditional mean and variance does not depend on the dimensions $d^{i,k}$ of the layers, which is why generic initialization methods scale the initial distribution by $s_k \propto \frac{1}{\sqrt{d^{i,k-1}}}$.

Problem. Unfortunately, this generic initialization approach can dramatically fail for MVNNs: For any non-zero initialization, the non-negativity constraint of the weights implies that the mean $\mu_k > 0$. This implies that the mean of a pre-activated neuron in the first hidden layer is $\mathbb{E} [(W^{i,1}x)_j] = d^{i,0} \mu_1 \bar{x}$. For a generic scaling s_k one would obtain $\mu_k \propto \frac{1}{\sqrt{d^{i,k-1}}}$ and thus the mean $\mathbb{E} [(W^{i,1}x)_j] \propto d^{i,0} \frac{1}{\sqrt{d^{i,0}}} \bar{x} = \sqrt{d^{i,0}} \bar{x}$ of the pre-activated

⁶We assume that the biases $b^{i,k} = 0$ are all initialized to zero throughout Section 3.2 to keep the notation simpler, while we formulate everything for the general case including random biases in Appendix E and in our code.

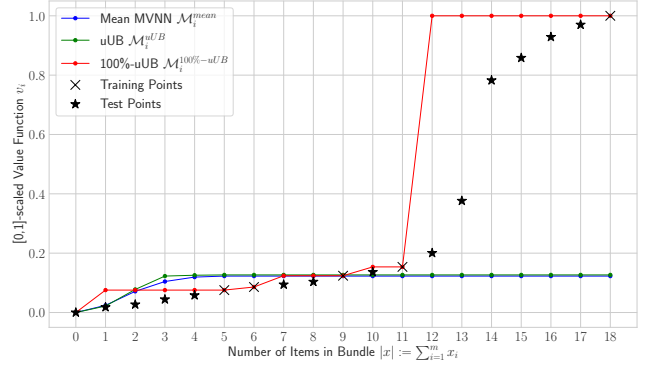


Figure 3: In contrast to our proposed initialization (see Figure 2), training fails with generic initialization already for relatively small [64,64]-architectures that were used here.

neurons diverges to infinity with a rate of $\sqrt{d^{i,0}}$ as $d^{i,0} \rightarrow \infty$. Analogously, the pre-activated neurons of every layer diverge to infinity as $d^{i,k-1} \rightarrow \infty$. This is particularly problematic for bReLU (as used in MVNNs) as their gradient is zero on $[0, t^{i,k}]^c$. Figure 3 shows that both MVNNs $\mathcal{M}_i^{\text{mean}}$ and $\mathcal{M}_i^{\text{uUB}}$ get “stuck.” This happens because already at initialization, every neuron in the first hidden layer has a pre-activation that is larger than $t^{i,1}$ for every training point.

This could be solved by scaling down the initial weights even more, e.g., $W_{j,l}^{i,k} \sim \text{Unif}[0, \frac{2}{d^{i,k-1}}]$ resulting in $\mu_k = \frac{1}{d^{i,k-1}}$. However, since for $W_{j,l}^{i,k} \sim \text{Unif}[0, \frac{2}{d^{i,k-1}}]$ it holds that $\sigma_k^2 \propto \frac{1}{(d^{i,k-1})^2}$, this induces a new problem of vanishing conditional variance $\mathbb{V} [(W^{i,k} z^{i,k-1})_j | z^{i,k-1}]$ with a rate of $\mathcal{O}(\frac{1}{d^{i,k-1}})$ for wide (i.e., $d^{i,k-1}$ large) MVNNs. Overall, it is impossible to simultaneously solve both problems by just scaling the distribution by a factor s_k , because the conditional mean $\mathbb{E} [(W^{i,k} z^{i,k-1})_j | z^{i,k-1}]$ scales with $s_k \cdot d^{i,k-1}$ and the conditional variance $\mathbb{V} [(W^{i,k} z^{i,k-1})_j | z^{i,k-1}]$ scales with $s_k^2 \cdot d^{i,k-1}$. Thus, for wide MVNNs, one of those two problems (i.e., either diverging expectation or vanishing variance) would persist.

Solution. We introduce a new initialization method that solves *both* problems at the same time. For this, we propose an i.i.d. mixture distribution of two different uniform distributions. For each weight, with probability $(1 - p_k)$ we sample from $\text{Unif}[0, A_k]$, and with probability p_k we sample from $\text{Unif}[0, B_k]$. If we choose p_k and A_k small enough, we can get arbitrarily small μ_k while not reducing σ_k too much. In Appendix E, we provide formulas for how to choose A_k, B_k and p_k depending on $d^{i,k-1}$. In Theorem 3 in Appendix E, we prove that, if the parameters are chosen in this way, then the conditional mean and conditional variance do not explode or vanish with increasing $d^{i,k-1}$ but stay constant for large $d^{i,k-1}$. Note that, in Figure 2, for $\mathcal{M}_i^{\text{mean}}$ and $\mathcal{M}_i^{\text{uUB}}$, we used our proposed initialization method for suitable A_k, B_k and p_k , such that the problem induced by a

generic initialization from Figure 3 is resolved.

3.3 Mixed Integer Linear Program (MILP)

A key step in ML-powered iterative combinatorial assignment mechanisms is finding the (predicted) social welfare-maximizing allocation, i.e., solving the *ML-based WDP*. Thus, a key requirement posed on any acquisition function \mathcal{A} in such a mechanism is to be able to efficiently solve $\max_{a \in \mathcal{F}} \mathcal{A}(a)$. Recall that, to define our acquisition function \mathcal{A} , we use $\mathcal{A} = \sum_{i \in N} \mathcal{A}_i(a_i)$ where the \mathcal{A}_i 's are bidder-specific upper uncertainty bounds. Thus, the ML-based WDP becomes

$$\max_{a \in \mathcal{F}} \sum_{i \in N} \mathcal{A}_i(a_i). \quad (10)$$

Weissteiner et al. (2022a) proposed a MILP for MVNNs with $\mathcal{A}_i := \mathcal{M}_i^\theta$ to efficiently solve eq. (10). Their MILP was based on a reformulation of the $\min(\cdot, \cdot)$ and $\max(\cdot, \cdot)$ in the bReLU activation $\min(\max(\cdot, 0), t)$. Thus, it required twice the number of binary variables *and* linear constraints as for a plain ReLU-NN. Since we use an MVNN-based uUB $\mathcal{A}_i := \mathcal{M}_i^{\text{uUB}}$ to define our acquisition function, we could directly use their MILP formulation. However, instead, we propose a new MILP, which is significantly more succinct. For this, let $o^{i,k} := W^{i,k} z^{i,k-1} + b^{i,k}$ be the *pre-activated* output and $z^{i,k} := \varphi_{0,t^{i,k}}(o^{i,k})$ be the output of the k^{th} layer with $l^{i,k} \leq o^{i,k} \leq u^{i,k}$, where the tight lower (upper) bound $l^{i,k}$ ($u^{i,k}$) is derived by forward-propagating the empty (full) bundle (Weissteiner et al. 2022a, Fact 1). In Theorem 2, we state our new MILP (see Appendix F.1 for the proof).⁷

Theorem 2 (MVNN MILP Tailored to Combinatorial Assignment). *Let $\mathcal{A}_i = \mathcal{M}_i^{\text{uUB}}$ be our MVNN-based uUBs. The ML-based WDP (10) can be formulated as the following MILP:*

$$\max_{a \in \mathcal{F}, z^{i,k}, \alpha^{i,k}, \beta^{i,k}} \left\{ \sum_{i \in N} W^{i,K_i} z^{i,K_i-1} \right\} \quad (11)$$

s.t. for $i \in N$ and $k \in \{1, \dots, K_i - 1\}$

$$z^{i,0} = a_i \quad (12)$$

$$z^{i,k} \leq \alpha^{i,k} \cdot t^{i,k} \quad (13)$$

$$z^{i,k} \leq o^{i,k} - l^{i,k} \cdot (1 - \alpha^{i,k}) \quad (14)$$

$$z^{i,k} \geq \beta^{i,k} \cdot t^{i,k} \quad (15)$$

$$z^{i,k} \geq o^{i,k} + (t^{i,k} - u) \beta^{i,k} \quad (16)$$

$$\alpha^{i,k} \in \{0, 1\}^{d^{i,k}}, \beta^{i,k} \in \{0, 1\}^{d^{i,k}} \quad (17)$$

Note that for each neuron of $\mathcal{A}_i = \mathcal{M}_i^{\text{uUB}}$, our new MILP has only 4 linear constraints, i.e., respective components of eqs. (13) to (16), compared to 8 in (Weissteiner et al. 2022a). Moreover, in contrast to the MILP in (Weissteiner et al. 2022a), our MILP does not make use of any “big-M” constraints, which are known to be numerically unstable.

⁷All vector inequalities should be understood component-wise.

4 Experiments

In this section, we experimentally evaluate the performance of BOCA in the CA domain. To this end, we equip the MLCA mechanism (see Section 2.2) with our new acquisition function $\mathcal{A} = \sum_{i \in N} \mathcal{M}_i^{\text{uUB}}$. We compare the efficiency of BOCA against the previously proposed MVNN-based and NN-based MLCA from (Weissteiner et al. 2022a) which do not explicitly model the mechanism’s uncertainty over values for not yet elicited bundles.⁸ We use our new parameter initialization method (Section 3.2) for $\mathcal{M}_i^{\text{uUB}}$, and we use our new MILP (Theorem 2) for solving the corresponding WDPs.

Experiment Setup. To generate synthetic CA instances, we use the following three domains from the spectrum auction test suite (SATS) (Weiss, Lubin, and Seuken 2017): LSVM, SRVM, and MRVM (see Appendix G.1 for details).⁹ SATS gives us access to the true optimal allocation a^* , which we use to measure the *efficiency loss*, i.e., $1 - V(a_R^*)/V(a^*)$ when eliciting reports R via MLCA. We report efficiency loss (and not revenue), as spectrum auctions are government-run, with a mandate to maximize welfare (Cramton 2013). See Appendix G.6 for a discussion of the corresponding results on revenue. To enable a fair comparison against prior work, for each domain, we use $Q^{\text{init}} = 40$ initial random queries (including the full bundle for the calculation of $\mathcal{M}_i^{100\%-\text{uUB}}$) and set the query budget to $Q^{\text{max}} = 100$ (see Appendix G.8 for results for $Q^{\text{init}} = 20$). We terminate any mechanism in an intermediate iteration if it already found an allocation with 0% efficiency loss.

Hyperparameter Optimization (HPO). We use *random search* (RS) (Bergstra and Bengio 2012) to optimize the hyperparameters of the mean MVNN $\mathcal{M}_i^{\text{mean}}$ and of our MVNN-based uUB $\mathcal{M}_i^{\text{uUB}}$. The HPO includes the NN-architecture parameters, training parameters such as learning rate, NOMU parameters, and initialization parameters (see Section 3.2). RS was carried out independently for each bidder type and SATS domain with a budget of 500 configurations, where each configuration was evaluated on 100 SATS instances. For each instance, the MVNNs $\mathcal{M}_i^{\text{mean}}$ and $\mathcal{M}_i^{\text{uUB}}$ were trained on uniformly at random chosen bundle-value pairs D^{train} and evaluated on a disjoint test set of different bundle-value pairs D^{test} . To select the winner configuration, we consider as evaluation metric the quantile-loss on the test set *and* the MAE on the training set, i.e., for each configuration and instance we calculate

$$|D^{\text{test}}|^{-1} \sum_{(x,y) \in D^{\text{test}}} \max\{(y - \mathcal{M}_i^{\text{uUB}}(x))q, (\mathcal{M}_i^{\text{uUB}}(x) - y)(1-q)\} + \text{MAE}(D^{\text{train}}), \quad (18)$$

which we then average over all 100 instances. We used four quantile parameters $q \in \{0.6, 0.75, 0.9, 0.95\}$ in eq. (18)

⁸In these methods, uncertainty over not yet elicited bundles is only modeled via the retraining of the (MV)NNs in each round, i.e., the random parameter initialization of the (MV)NNs. This can be seen as simple form of Thompson sampling (see last paragraph in Appendix C).

⁹We do not use GSVM, as Weissteiner et al. (2022a) already achieved 0% efficiency loss in GSVM via MVNN-based MLCA.

DOMAIN	Q^{\max}	EFFICIENCY LOSS IN % ↓				T-TEST FOR EFFICIENCY:		
		BOCA	WEISSTEINER ET AL. (2022A) MVNN-MLCA	WEISSTEINER AND SEUKEN (2020) NN-MLCA	WEISSTEINER ET AL. (2022B) FT-MLCA	RS	$\mathcal{H}_0 : \mu_{\text{MVNN-MLCA}} \leq \mu_{\text{BOCA}}$	$\mathcal{H}_0 : \mu_{\text{NN-MLCA}} \leq \mu_{\text{BOCA}}$
LSVM	100	0.39 ± 0.30	00.70 ± 0.40	02.91 ± 1.44	01.54 ± 0.65	31.73 ± 2.15	$p_{\text{VAL}} = 9e-2$	$p_{\text{VAL}} = 3e-4$
SRVM	100	0.06 ± 0.02	00.23 ± 0.06	01.13 ± 0.22	00.72 ± 0.16	28.56 ± 1.74	$p_{\text{VAL}} = 5e-6$	$p_{\text{VAL}} = 2e-13$
MRVM	100	7.77 ± 0.34	08.16 ± 0.41	09.05 ± 0.53	10.37 ± 0.57	48.79 ± 1.13	$p_{\text{VAL}} = 8e-2$	$p_{\text{VAL}} = 2e-5$

Table 1: BOCA vs MVNN-MLCA, NN-MLCA, Fourier transform (FT)-MLCA and random search (RS). Shown are averages and a 95% CI on a test set of 50 instances. Winners based on a t-test with significance level of 1% are marked in grey.

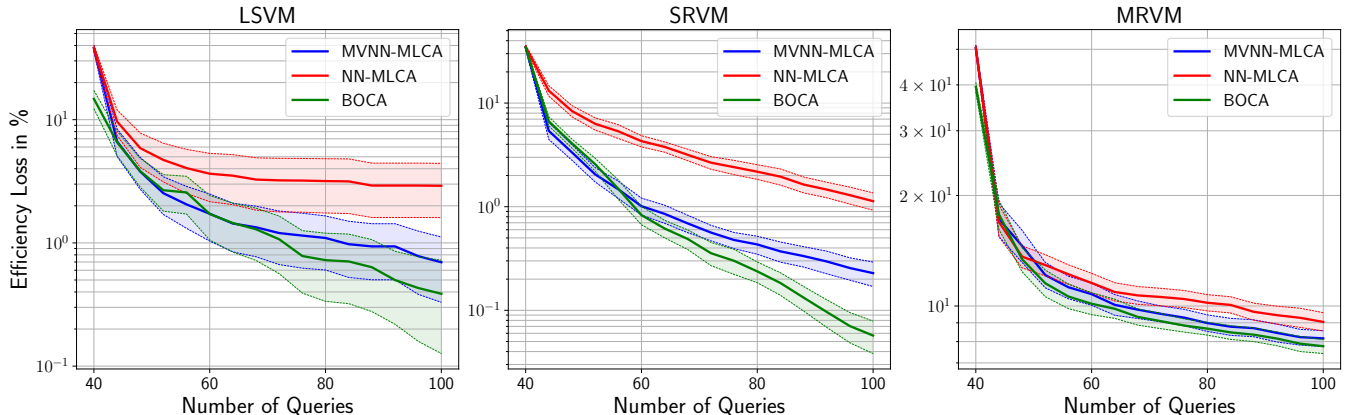


Figure 4: Efficiency loss paths (i.e., regret plots) of BOCA compared to the results from Weissteiner et al. (2022a) of MVNN-MLCA and NN-MLCA without any notion of uncertainty. Shown are averages with 95% CIs over 50 CA instances.

to achieve different levels of exploration (i.e., the resulting uUBs become larger the more we increase q in eq. (18)). This evaluation metric *simultaneously* measures the quality of the uUB on the test data (via the first term, i.e., the q -loss) as well as the quality of the uUB predictions on the training data (via the second term, i.e., the MAE). For each quantile q and SATS domain, we then proceed with the winner configuration of $\mathcal{M}_i^{\text{uUB}}$ and evaluate the efficiency of BOCA on a separate set of 50 instances. Details on hyperparameter ranges and the training procedure are provided in Appendices G.2 and G.3.

Results. In Table 1, we show the average efficiency loss of each approach after $Q^{\max} = 100$ queries (see Appendix G.5 for more detailed results). We observe that our proposed BOCA outperforms MVNN-based MLCA (MVNN-MLCA) on the SRVM domain in a statistically significant way, and it performs on-par in LSVM and MRVM, with a slightly better average performance. Given that MVNNs previously achieved SOTA performance, we also outperform the other benchmarks (i.e., NN and FT-MLCA). The poor performance of RS highlights the intrinsic difficulty of this task. Note that the amount of exploration needed is domain dependent, which explains why BOCA outperforms MVNN-MLCA in some but not all domains. However, our results also show that using an uUB (as in BOCA) instead of just a mean prediction (as in MVNN-MLCA) does not hurt.

Figure 4 shows the efficiency loss path for all domains. We see that the superior (average) performance of $\mathcal{M}_i^{\text{uUB}}$ does not only hold at the end of the auction (at $Q^{\max} = 100$),

but also for a large range of queries: in LSVM, BOCA is better for [70,100]; in SRVM, BOCA is significantly better for [70,100]; in MRVM, BOCA is better for [0,100] (see Appendix G.6 for results on revenue where BOCA significantly outperforms SOTA also for MRVM). In Appendix G.7, we study to what degree BOCA’s performance increase is due to (a) our uncertainty model (Section 3.1) versus (b) our new parameter initialization method (Section 3.2). Finally, in Appendix G.8, we provide further results for a reduced number of $Q^{\text{init}} = 20$ initial queries, where we see that integrating uncertainty becomes even more beneficial.

5 Conclusion

In this paper, we have proposed a Bayesian optimization-based combinatorial assignment (BOCA) mechanism. On a conceptual level, our main contribution was the integration of model uncertainty over agents’ preferences into ML-based preference elicitation. On a technical level, we have designed a new method for estimating an upper uncertainty bound that exploits the monotonicity of agents’ preferences in the combinatorial assignment domain and the finite nature of this setting. Our experiments have shown that BOCA performs as good or better than the SOTA in terms of efficiency. An interesting direction for future work is the evaluation of BOCA in other combinatorial assignment domains, such as combinatorial exchanges or course allocation (e.g., see (Soumalias et al. 2022)). Finally, it would also be interesting to apply BOCA’s conceptual idea in the combinatorial BO settings outside of combinatorial assignment.

Acknowledgments

We thank the anonymous reviewers for helpful comments. This paper is part of a project that has received funding from the European Research Council (ERC) under the European Union’s Horizon 2020 research and innovation program (Grant agreement No. 805542).

References

- Ausubel, L.; and Cramton, P. 2011. Auction design for wind rights. *Report to Bureau of Ocean Energy Management, Regulation and Enforcement*. 1
- Ausubel, L. M.; and Baranov, O. 2017. A practical guide to the combinatorial clock auction. *Economic Journal*, 127(605): F334–F350. 1, 23
- Ausubel, L. M.; Cramton, P.; and Milgrom, P. 2006. The clock-proxy auction: A practical combinatorial auction design. In Cramton, P.; Shoham, Y.; and Steinberg, R., eds., *Combinatorial Auctions*, 115–138. MIT Press. 1
- Bergstra, J.; and Bengio, Y. 2012. Random search for hyperparameter optimization. *Journal of machine learning research*, 13(2). 7
- Bichler, M.; Fux, V.; and Goeree, J. K. 2019. Designing combinatorial exchanges for the reallocation of resource rights. *Proceedings of the National Academy of Sciences*, 116(3): 786–791. 1
- Blundell, C.; Cornebise, J.; Kavukcuoglu, K.; and Wierstra, D. 2015. Weight uncertainty in neural networks. In *32nd International Conference on Machine Learning (ICML)*. 2
- Bonilla, E. V.; Guo, S.; and Sanner, S. 2010. Gaussian process preference elicitation. *Advances in neural information processing systems*, 23. 2
- Brero, G.; Lubin, B.; and Seuken, S. 2018. Combinatorial Auctions via Machine Learning-based Preference Elicitation. In *Proceedings of the 27th International Joint Conference on Artificial Intelligence*. 1
- Brero, G.; Lubin, B.; and Seuken, S. 2021. Machine Learning-powered Iterative Combinatorial Auctions. *arXiv preprint arXiv:1911.08042*. 1, 2, 3, 11, 12
- Budish, E. 2011. The combinatorial assignment problem: Approximate competitive equilibrium from equal incomes. *Journal of Political Economy*, 119(6): 1061–1103. 1
- Chapelle, O.; and Li, L. 2011. An Empirical Evaluation of Thompson Sampling. In *NIPS*. 3
- Cramton, P. 2013. Spectrum auction design. *Review of Industrial Organization*, 42(2): 161–190. 1, 7
- De Ath, G.; Everson, R. M.; Rahat, A. A.; and Fieldsend, J. E. 2021. Greed is good: Exploration and exploitation trade-offs in Bayesian optimisation. *ACM Transactions on Evolutionary Learning and Optimization*, 1(1): 1–22. 25
- Frazier, P. I. 2018. A tutorial on Bayesian optimization. *arXiv preprint arXiv:1807.02811*. 3
- Gal, Y.; and Ghahramani, Z. 2016. Dropout as a Bayesian Approximation: Representing Model Uncertainty in Deep Learning. In *33rd International Conference on Machine Learning (ICML)*, 1050–1059. 2, 14
- Goeree, J. K.; and Holt, C. A. 2010. Hierarchical package bidding: A paper & pencil combinatorial auction. *Games and Economic Behavior*, 70(1): 146–169. 21
- Graves, A. 2011. Practical variational inference for neural networks. In *Advances in neural information processing systems*, 2348–2356. 2
- Heiss, J.; Weissteiner, J.; Wutte, H.; Seuken, S.; and Teichmann, J. 2022. NOMU: Neural Optimization-based Model Uncertainty. In *Proceedings of the 39th International Conference on Machine Learning (ICML)*. 2, 4, 5, 12, 13, 14, 15, 16, 21
- Hernández-Lobato, J. M.; and Adams, R. 2015. Probabilistic backpropagation for scalable learning of bayesian neural networks. In *International Conference on Machine Learning*, 1861–1869. 2
- Kandasamy, K.; Dasarathy, G.; Schneider, J.; and Póczos, B. 2017. Multi-fidelity bayesian optimisation with continuous approximations. In *International Conference on Machine Learning*, 1799–1808. PMLR. 2
- Kuleshov, V.; Fenner, N.; and Ermon, S. 2018. Accurate Uncertainties for Deep Learning Using Calibrated Regression. In *Proceedings of the 35th International Conference on Machine Learning*, 2796–2804. PMLR. 14, 15
- Lakshminarayanan, B.; Pritzel, A.; and Blundell, C. 2017. Simple and scalable predictive uncertainty estimation using deep ensembles. In *Advances in neural information processing systems*, 6402–6413. 2, 12, 14, 15
- Nisan, N.; and Segal, I. 2006. The communication requirements of efficient allocations and supporting prices. *Journal of Economic Theory*, 129(1): 192–224. 1
- Ober, S. W.; and Rasmussen, C. E. 2019. Benchmarking the neural linear model for regression. *arXiv preprint arXiv:1912.08416*. 2
- Papalexopoulos, P.; Tjandraatmadja, C.; Anderson, R.; Vielma, J. P.; and Belanger, D. 2022. Constrained Discrete Black-Box Optimization using Mixed-Integer Programming. In *Proceedings of the 39th International Conference on Machine Learning*, 17295–17322. PMLR. 12, 13
- Sandholm, T.; and Boutilier, C. 2006. Preference elicitation in combinatorial auctions. *Combinatorial auctions*, 10. 1
- Scheffel, T.; Ziegler, G.; and Bichler, M. 2012. On the impact of package selection in combinatorial auctions: an experimental study in the context of spectrum auction design. *Experimental Economics*, 15(4): 667–692. 21
- Soumalias, E.; Zamanlooy, B.; Weissteiner, J.; and Seuken, S. 2022. Machine Learning-powered Course Allocation. *arXiv:2210.00954*. 8
- Srinivas, N.; Krause, A.; Kakade, S. M.; and Seeger, M. W. 2012. Information-Theoretic Regret Bounds for Gaussian Process Optimization in the Bandit Setting. *IEEE Transactions on Information Theory*, 58(5): 3250–3265. 3
- Weiss, M.; Lubin, B.; and Seuken, S. 2017. Sats: A universal spectrum auction test suite. In *Proceedings of the 16th Conference on Autonomous Agents and MultiAgent Systems*, 51–59. 5, 7, 21

Weissteiner, J.; Heiss, J.; Siems, J.; and Seuken, S. 2022a. Monotone-Value Neural Networks: Exploiting Preference Monotonicity in Combinatorial Assignment. In *Proceedings of the 31st International Joint Conference on Artificial Intelligence*. 2, 3, 4, 7, 8, 12, 13, 19, 20, 21, 23, 24

Weissteiner, J.; Heiss, J.; Siems, J.; and Seuken, S. 2023. Bayesian Optimization-based Combinatorial Assignment. In *Proceedings of the 37th AAAI Conference of Artificial Intelligence (forthcoming)*. 1

Weissteiner, J.; and Seuken, S. 2020. Deep Learning-powered Iterative Combinatorial Auctions. In *Proceedings of the 34th AAAI Conference of Artificial Intelligence*, 2284–2293. 2, 8, 12, 13

Weissteiner, J.; Wendler, C.; Seuken, S.; Lubin, B.; and Püschel, M. 2022b. Fourier Analysis-based Iterative Combinatorial Auctions. In *Proceedings of the 31st International Joint Conference on Artificial Intelligence*. 2, 8

Wenzel, F.; Snoek, J.; Tran, D.; and Jenatton, R. 2020. Hyperparameter ensembles for robustness and uncertainty quantification. *arXiv preprint arXiv:2006.13570*. 2

Appendix

Bayesian Optimization-based Combinatorial Assignment

A A Machine Learning-powered ICA

In this section, we present in detail the *machine learning-powered combinatorial auction (MLCA)* by Brero, Lubin, and Seuken (2021).

At the core of MLCA is a *query module* (Algorithm 1), which, for each bidder $i \in I \subseteq N$, determines a new value query q_i . First, in the *estimation step* (Line 1), an ML algorithm \mathcal{A}_i is used to learn bidder i 's valuation from reports R_i . Next, in the *optimization step* (Line 2), an *ML-based WDP* is solved to find a candidate q of value queries. In principle, any ML algorithm \mathcal{A}_i that allows for solving the corresponding ML-based WDP in a fast way could be used. Finally, if q_i has already been queried before (Line 4), another, more restricted ML-based WDP (Line 6) is solved and q_i is updated correspondingly. This ensures that all final queries q are new.

Algorithm 1: NEXTQUERIES(I, R) (Brero et al. 2021)

Inputs: Index set of bidders I and reported values R

```

1 foreach  $i \in I$  do Fit  $\mathcal{A}_i$  on  $R_i$ :  $\mathcal{A}_i[R_i]$   $\triangleright$  Estimation step
2 Solve  $q \in \operatorname{argmax}_{a \in \mathcal{F}} \sum_{i \in I} \mathcal{A}_i[R_i](a_i)$   $\triangleright$  Optimization step
3 foreach  $i \in I$  do
4   if  $(q_i, \hat{v}_i(q_i)) \in R_i$  then  $\triangleright$  Bundle already queried
5     Define  $\mathcal{F}' = \{a \in \mathcal{F} : a_i \neq x, \forall (x, \hat{v}_i(x)) \in R_i\}$ 
6     Re-solve  $q' \in \operatorname{argmax}_{a \in \mathcal{F}'} \sum_{l \in I} \mathcal{A}_l[R_l](a_l)$ 
7     Update  $q_i = q'_i$ 
8   end
9 end
10 return Profile of new queries  $q = (q_1, \dots, q_n)$ 

```

In Algorithm 2, we present MLCA. In the following, let $R_{-i} = (R_1, \dots, R_{i-1}, R_{i+1}, \dots, R_n)$. MLCA proceeds in rounds until a maximum number of queries per bidder Q^{\max} is reached. In each round, it calls Algorithm 1 ($Q^{\text{round}} - 1$) $n + 1$ times: for each bidder $i \in N$, $Q^{\text{round}} - 1$ times excluding a different bidder $j \neq i$ (Lines 5–10, sampled *marginal economies*) and once including all bidders (Line 11, *main economy*). In total each bidder is queried Q^{round} bundles per round in MLCA. At the end of each round, the mechanism receives reports R^{new} from all bidders for the newly generated queries q^{new} and updates the overall elicited reports R (Lines 12–14). In Lines 16–17, MLCA computes an allocation a_R^* that maximizes the *reported* social welfare (see Equation (1)) and determines VCG payments $p(R)$ based on the reported values R (see Appendix Definition B.1).

In this paper, we consider the following two minor adaptations of the generic MLCA mechanism described above:

1. **Balanced and global marginal economies:** In Lines 5–6 of Algorithm 2, MLCA draws for each bidder $i \in N$ uniformly at random a set of marginal economies \tilde{N} to generate queries in this marginal economy. However, this implies that at the end of the auction it only holds on average that the same number of queries is asked from

Algorithm 2: MLCA($Q^{\text{init}}, Q^{\max}, Q^{\text{round}}$) (Brero et al. 2021)

Params: $Q^{\text{init}}, Q^{\max}, Q^{\text{round}}$ initial, max and #queries/round

```

1 foreach  $i \in N$  do
2   | Receive reports  $R_i$  for  $Q^{\text{init}}$  randomly drawn bundles
3 end
4 for  $k = 1, \dots, \lfloor (Q^{\max} - Q^{\text{init}}) / Q^{\text{round}} \rfloor$  do  $\triangleright$  Round iterator
5   | foreach  $i \in N$  do  $\triangleright$  Marginal economy queries
6     | Draw uniformly without replacement ( $Q^{\text{round}} - 1$ )
7       | bidders from  $N \setminus \{i\}$  and store them in  $\tilde{N}$ 
8       | foreach  $j \in \tilde{N}$  do
9         | |  $q^{\text{new}} = q^{\text{new}} \cup \text{NextQueries}(N \setminus \{j\}, R_{-j})$ 
10        | end
11     |  $q^{\text{new}} = \text{NextQueries}(N, R)$   $\triangleright$  Main economy queries
12     | foreach  $i \in N$  do
13       | Receive reports  $R_i^{\text{new}}$  for  $q_i^{\text{new}}$ , set  $R_i = R_i \cup R_i^{\text{new}}$ 
14     | end
15 end
16 Given elicited reports  $R$  compute  $a_R^*$  as in Equation (1)
17 Given elicited reports  $R$  compute VCG-payments  $p(R)$ 
18 return Final allocation  $a_R^*$  and payments  $p(R)$ 

```

each bidder in each marginal economy. Moreover, since \tilde{N} is re-drawn for each bidder this creates a computational overhead, since typically the WDPs in Line 8 in *NextQueries* needs to be solved more often. For example consider the case $N = \{1, 2, 3, 4, 5, 6\}$, $Q^{\text{round}} = 3$ and that for bidder 1 the $Q^{\text{round}} - 1 = 2$ sampled marginal economies were given as $\tilde{N} = \{3, 4\}$, whilst for bidder 2, $\tilde{N} = \{5, 6\}$, and for bidder 3, $\tilde{N} = \{1, 2\}$. In this case, the WDPs in *NextQueries* would need to be solved 6 times, which is the maximum possible. In our implementation, we change the following two things: First, we reduce the computational overhead by once globally selecting Q^{round} marginal economies in each iteration, i.e., we select a set $\tilde{N}_{\text{global}}$ consisting of Q^{round} marginal economies before Line 5, and then select \tilde{N} for each bidder $i \in N$ in the loop in Line 5 as admissible subset of size $Q^{\text{round}} - 1$ of $\tilde{N}_{\text{global}}$. In the above example, if $\tilde{N}_{\text{global}} = \{3, 4, 1\}$, then this ensures that only $Q^{\text{round}} = 3$ WDPs in the marginal economies are solved in one iteration. Second, we do not determine $\tilde{N}_{\text{global}}$ uniformly at random, but ensure that at the end of the auction each marginal economy was selected equally often up to a difference in counts of at most one.

2. **Single training per iteration:** To further reduce computational overhead, we train each bidder's ML algorithm \mathcal{A}_i once at the beginning of each iteration, and then only select in *NextQueries* the trained \mathcal{A}_i corresponding to the active set of bidders I . This reduces the amount of total training procedures per iteration from (worst case) n^2 to n .

B Incentives of MLCA

In this section, we review the key arguments by Brero, Lubin, and Seuken (2021) why MLCA has good incentives in practice. First, we define VCG-payments given bidder's re-

ports.

Definition B.1. (VCG PAYMENTS FROM REPORTS) Let $R = (R_1, \dots, R_n)$ denote an elicited set of reported bundle-value pairs from each bidder obtained from MLCA (Algorithm 2) and let $R_{-i} := (R_1, \dots, R_{i-1}, R_{i+1}, \dots, R_n)$. We then calculate the VCG payments $p(R) = (p(R)_1, \dots, p(R)_n) \in \mathbb{R}_+^n$ as follows:

$$p(R)_i := \sum_{j \in N \setminus \{i\}} \hat{v}_j \left((a_{R_{-i}}^*)_j \right) - \sum_{j \in N \setminus \{i\}} \hat{v}_j \left((a_R^*)_j \right). \quad (19)$$

where $a_{R_{-i}}^*$ maximizes the reported social welfare (SW) when excluding bidder i , i.e.,

$$a_{R_{-i}}^* \in \operatorname{argmax}_{a \in \mathcal{F}} \widehat{V}(a | R_{-i}) = \operatorname{argmax}_{a \in \mathcal{F}} \sum_{\substack{j \in N \setminus \{i\}; \\ (a_j, \hat{v}_j(a_j)) \in R_j}} \hat{v}_j(a_j), \quad (20)$$

and a_R^* is a reported-social-welfare-maximizing allocation (including all bidders), i.e.,

$$a_R^* \in \operatorname{argmax}_{a \in \mathcal{F}} \widehat{V}(a | R) = \operatorname{argmax}_{a \in \mathcal{F}} \sum_{i \in N: (a_i, \hat{v}_i(a_i)) \in R_i} \hat{v}_i(a_i). \quad (21)$$

Therefore, when using VCG, bidder i 's utility is:

$$\begin{aligned} u_i &= v_i((a_R^*)_i) - p(R)_i \\ &= v_i((a_R^*)_i) + \underbrace{\sum_{j \in N \setminus \{i\}} \hat{v}_j((a_R^*)_j)}_{\text{(a) Reported SW of main economy}} - \underbrace{\sum_{j \in N \setminus \{i\}} \hat{v}_j((a_{R_{-i}}^*)_j)}_{\text{(b) Reported SW of marginal economy}}. \end{aligned}$$

Any beneficial misreport must increase the difference (a) – (b).

MLCA has two features that mitigate manipulations. First, MLCA explicitly queries each bidder's marginal economy (Algorithm 2, Line 5), which implies that (b) is practically independent of bidder i 's bid (Section 7.3 in (Brero, Lubin, and Seuken 2021) provides experimental support for this). Second, MLCA enables bidders to “push” information to the auction which they deem useful. This mitigates certain manipulations that target (a), as it allows bidders to increase (a) with truthful information. Brero, Lubin, and Seuken (2021) argue that any remaining manipulation would be implausible as it would require almost complete information.¹⁰

If we are willing to make two assumptions, we also obtain a theoretical incentive guarantee. Assumption 1 requires that, if all bidders bid truthfully, then MLCA finds an efficient allocation. Assumption 2 requires that, for all bidders i , if all other bidders report truthfully, then the social welfare of bidder i 's marginal economy is independent of his value reports. If both assumptions hold, then bidding truthfully is an ex-post Nash equilibrium in MLCA.

¹⁰In this paper, we propose a new method that uses a notion of epistemic uncertainty to actively explore regions of the bundle space with high uncertainty. Intuitively, this makes manipulation even harder, since additional exploration makes it more difficult for a bidder to prevent other bidders from getting queries in certain regions.

C BO Perspective of ICAs

In this section, we discuss the Bayesian optimization (BO) perspective of iterative combinatorial assignment. Specifically, we analyze the MLCA mechanism (see Section 2.2 for an overview or Appendix A for a detailed description) in the light of BO.

Iterative combinatorial assignment can be seen as a combinatorial BO task with an expensive-to-evaluate function:

- The objective (e.g., social welfare) in general lacks known structure and when evaluating it (e.g., value queries) one only observes the objective at a single input point and no derivatives such that gradient-based optimization cannot be used.
- Typically one can only query a very limited amount of information to find an approximately optimal allocation, For example, in a real-world spectrum auction, the auctioneer can only ask each bidder to answer on the order of 100 value queries for different bundles of items, even though the space of possible bundles is exponential in the number of items m , i.e., there are 2^m possible bundles and $(n+1)^m$ possible allocations.

C.1 BO Perspective of MLCA

In this paper, we extend prior work on MLCA with a notion of uncertainty that makes MLCA more similar to classic BO. Specifically, we now use an MVNN-based upper uncertainty bound (uUB) to define our acquisition function. This allows MLCA to trade-off exploration and exploitation making it more likely to find optimal allocations.

However, in addition to the challenges that arise in BO, combinatorial assignment adds their own set of challenges. For example, Gaussian Process-based BO often does not extend beyond 10-20 input dimension, which is problematic as in combinatorial assignment the input space can be much larger, e.g. for $m = 98$ items and $n = 10$ bidder the input space would be 980 dimensional (MRVM). In addition, integrality constraints to obtain only whole items (i.e., combinatorial assignment deals with assigning m indivisible items to agents) and feasibility constraints that ensure to allocate each item only once to a single agent are often only incorporated via rounding or randomization.

Our work addresses both problems by combining (MV)NN-based MLCA by (Weissteiner and Seuken 2020; Weissteiner et al. 2022a) with the recently introduced NOMU (Heiss et al. 2022), an optimization-based method to obtain uncertainty estimates for the prediction of NNs. Importantly, NOMU enables to represent an uUB as a *single* NN in contrast to other more expensive methods such as ensembles (Lakshminarayanan, Pritzel, and Blundell 2017). Thus, NOMU is particularly suited for iterative combinatorial assignment, where uUB-based WDPs are solved hundreds of times to generate informative queries.

Thompson Sampling Recently, Papalexopoulos et al. (2022) also proposed a MILP-based BO method using a ReLU NN as surrogate model and Thompson sampling as acquisition function. Concretely, Papalexopoulos et al. (2022) approximate Thompson sampling via retraining of

the NN from scratch with a new random initialization. Subsequently, they determine the next query by solving an NN-based MILP. However, unlike our proposal, Papalexopoulos et al. (2022) do only implicitly integrate a very limited notion of uncertainty, i.e., via a random parameter initialization of the NN, making their approach conceptually equivalent to the (MV)NN-based MLCA by (Weissteiner and Seuken 2020; Weissteiner et al. 2022a). In particular, this approximation of Thompson sampling only achieves sufficient exploration if the diversity induced by different random initialization seeds is large enough. However, Heiss et al. (2022, Remark B.5) showed that the diversity of an NN ensemble (in noiseless settings) is rather small and in (Heiss et al. 2022, Remark B.5) the ensemble’s uncertainty needed to be scaled up by a factor of ≈ 10 to make its uncertainty competitive. However, in Thompson sampling the desired amount of uncertainty/exploration cannot be easily calibrated/scaled. Moreover, our experimental results in spectrum auctions suggests that indeed the method by (Weissteiner et al. 2022a), which uses conceptually the same notion of uncertainty as in (Papalexopoulos et al. 2022), is outperformed by our proposal.

D NOMU for for Monotone NNs

In this section we give more details regarding our uncertainty estimates for monotonically increasing functions based on NOMU (see Section 3.1).

D.1 Proof of Theorem 1

The 100%-uUB $f^{100\%-uUB}(x) := \sup_{f \in \mathcal{H}_{D^{\text{train}}}} f(x)$ is defined via a 2^m -dimensional optimization problem with n^{train} constraints. In the following proof, we analytically derive the explicit closed-form joint solution of 2^m such optimization problems (one for each x), which we can represent as an MVNN that does not require any optimization algorithm.

Proof of Theorem 1. In the 1st part of the proof (which is based on the proof of Weissteiner et al. (2022a, Theorem 1)), we explicitly construct $\mathcal{M}_i^{100\%-uUB}$ and show that $\mathcal{M}_i^{100\%-uUB} \in \mathcal{V}_{D^{\text{train}}}$. Equation (26) gives our explicit (fast to evaluate) closed-form formula for $\mathcal{M}_i^{100\%-uUB}$, which can be directly written down without any training algorithm.

The 2nd part of the proof (which is new) shows that $\mathcal{M}_i^{100\%-uUB}$ is indeed the 100%-uUB by showing that it is maximal (and thus the supremum is actually a maximum).

- Let $\hat{v}_i \in \mathcal{V}$ and let $D^{\text{train}} = \{(x^{(l)}, \hat{v}_i(x^{(l)}))\}_{l=1}^{n^{\text{train}}}$ be a set of n^{train} observed training points corresponding to \hat{v}_i . First, given D^{train} , we construct an MVNN $\mathcal{M}_i^{100\%-uUB}$ with weights $\theta = (W_{D^{\text{train}}}^i, b_{D^{\text{train}}}^i)$ such that $\mathcal{M}_i^{100\%-uUB}(x) = f^{100\%-uUB}(x)$ for all $x \in \mathcal{X}$. Recall, that by definition $\hat{v}_i((0, \dots, 0)) = 0$ and that we assume that $((1, \dots, 1), \hat{v}_i((1, \dots, 1))) \in D^{\text{train}}$. Now let $(w_l)_{l=0}^{n^{\text{train}}}$ denote the observed/known values corresponding to \hat{v}_i sorted in increasing order, i.e. let $x^{(0)} = (0, \dots, 0)$ with

$$w_0 := \hat{v}_i(x^{(0)}) = 0, \quad (22)$$

let $x^{(n^{\text{train}})} = (1, \dots, 1)$ with

$$w_{n^{\text{train}}} := \hat{v}_i(x^{(n^{\text{train}})}), \quad (23)$$

and $x^{(j)}, x^{(k)} \in \mathcal{X} \setminus \{x^{(0)}, x^{(n^{\text{train}})}\}$ for $0 < j < k \leq n^{\text{train}} - 1$ with

$$w_j := \hat{v}_i(x^{(j)}) \leq w_k := \hat{v}_i(x^{(k)}). \quad (24)$$

In the following, we slightly abuse the notation and write for $x^{(j)}, x^{(k)} \in \mathcal{X}$, $x^{(j)} \subseteq x^{(k)}$ iff for the corresponding sets $A^j, A^k \in 2^M$ it holds that $A^j \subseteq A^k$. Furthermore, we denote by $\langle \cdot, \cdot \rangle$ the Euclidean scalar product on \mathbb{R}^m . Before we show that our construction fulfills $\mathcal{M}_i^{100\%-uUB} \in \mathcal{V}_{D^{\text{train}}}$, we define it as

$$\begin{aligned} \mathcal{M}_i^{100\%-uUB}(x) &:= \sum_{k=0}^{n^{\text{train}}-1} (w_{k+1} - w_k) \mathbb{1}_{\{\forall j \in \{0, \dots, k\} : x \not\subseteq x^{(j)}\}} \\ &= \sum_{k=0}^{n^{\text{train}}-1} (w_{k+1} - w_k) \varphi_{0,1} \left(\sum_{j=0}^k \varphi_{0,1} \left(\langle 1 - x^{(j)}, x \rangle \right) - k \right), \end{aligned} \quad (25)$$

$$(26)$$

where the second equality follows since

$$x \not\subseteq x^{(j)} \iff \langle 1 - x^{(j)}, x \rangle \geq 1 \quad (27)$$

$$\iff \varphi_{0,1} \left(\langle 1 - x^{(j)}, x \rangle \right) = 1, \quad (28)$$

which implies that

$$\forall j \in \{0, \dots, k\} : x \not\subseteq x^{(j)} \quad (29)$$

$$\iff \sum_{j=0}^k \varphi_{0,1} \left(\langle 1 - x^{(j)}, x \rangle \right) = k + 1, \quad (30)$$

and

$$\mathbb{1}_{\{\forall j \in \{0, \dots, k\} : x \not\subseteq x^{(j)}\}} = \varphi_{0,1} \left(\sum_{j=0}^k \varphi_{0,1} \left(\langle 1 - x^{(j)}, x \rangle \right) - k \right). \quad (31)$$

We now show that $\mathcal{M}_i^{100\%-uUB}$ is actually an MVNN. Equation (26) can be equivalently written in matrix notation as

$$\underbrace{\begin{bmatrix} w_1 - w_0 \\ w_2 - w_1 \\ \vdots \\ w_{n^{\text{train}}} - w_{n^{\text{train}}-1} \end{bmatrix}}_{(W_{D^{\text{train}}}^{i,3})^\top \in \mathbb{R}_{\geq 0}^{n^{\text{train}}}} \varphi_{0,1} \left(W_{D^{\text{train}}}^{i,2} \varphi_{0,1} \left(\underbrace{\begin{bmatrix} 1 - x^{(1)} \\ 1 - x^{(2)} \\ \vdots \\ 1 - x^{(n^{\text{train}})} \end{bmatrix}}_{W_{D^{\text{train}}}^{i,1} \in \mathbb{R}_{\geq 0}^{(n^{\text{train}}) \times m}} x \right) + \underbrace{\begin{bmatrix} 0 \\ -1 \\ \vdots \\ -(n^{\text{train}} - 1) \end{bmatrix}}_{b_{D^{\text{train}}}^{i,2} \in \mathbb{R}_{\leq 0}^{n^{\text{train}}}} \right)$$

with $W_{D^{\text{train}}}^{i,2} \in \mathbb{R}_{\geq 0}^{(n^{\text{train}}) \times (n^{\text{train}})}$ a lower triangular matrix of ones, i.e.,

$$W_{D^{\text{train}}}^{i,2} := \begin{bmatrix} 1 & 0 & \dots & 0 \\ \vdots & \ddots & \ddots & \vdots \\ \vdots & & \ddots & 0 \\ \vdots & & & 1 \end{bmatrix}.$$

From that, we can see that $\mathcal{M}_i^{100\%-uUB}$ is indeed an MVNN with four layers in total (i.e., two hidden layers) and respective dimensions $[m, n^{\text{train}}, n^{\text{train}}, 1]$. From Equation (25) we can see that for all $l = 0, \dots, n^{\text{train}}$: $\mathcal{M}_i^{100\%-uUB}(x^{(l)}) = \hat{v}_i(x^{(l)})$ and therefore $\mathcal{M}_i^{100\%-uUB} \in \mathcal{V}_{D^{\text{train}}}$.

- Now we have to check what happens for $x \in \mathcal{X}$: $(x, \hat{v}_i(x)) \notin D^{\text{train}}$. Therefore, let $x \in \mathcal{X}$: $(x, \hat{v}_i(x)) \notin D^{\text{train}}$. Then, by definition we get that $\mathcal{M}_i^{100\%-uUB}(x) = w_k$, where $k \in \{0, \dots, n^{\text{train}}\}$ is the smallest integer such that $x \subseteq x^{(k)}$. Assume there exists an $h \in \mathcal{V}_{D^{\text{train}}}$ with $h(x) > \mathcal{M}_i^{100\%-uUB}(x) = w_k = h(x^{(k)})$. However, since $x \subseteq x^{(k)}$ this is a contradiction to h fulfilling the monotonicity property. Thus, we get that $\mathcal{M}_i^{100\%-uUB}(x) = \max_{f \in \mathcal{V}_{D^{\text{train}}}} f(x)$. Since x was chosen arbitrarily, we finally get that $\mathcal{M}_i^{100\%-uUB}(x) = \max_{f \in \mathcal{V}_{D^{\text{train}}}} f(x)$ for all $x \in \mathcal{X}$ which concludes the proof. \square

D.2 ICA-based New NOMU Architecture

In this section, we provide more details on our carefully chosen ICA-based new NOMU architecture. The original NOMU architecture from (Heiss et al. 2022) outputs a mean prediction \hat{f} , which is in our case the mean-MVNN $\mathcal{M}_i^{\text{mean}}$ and a model uncertainty prediction $\hat{\sigma}_f$. Then, uUBs in the original NOMU algorithm at an input point x are defined as $\hat{f}(x) + c \cdot \hat{\sigma}_f(x)$.

Monotone uUBs and Non-Monotone $\hat{\sigma}_f$

Monotone Value Functions Imply Monotone uUBs. Knowing that the unknown ground truth function is monotonically increasing¹¹ means that the support of the prior in function space only contains monotonically increasing functions in Bayesian language. In frequentist language this means that the hypothesis class \mathcal{H} only contains monotonically increasing functions. In both cases the resulting uUBs are monotonically increasing too, which we next prove in Propositions 1 and 2.

Proposition 1. *Let $\mathbb{P}[f \text{ is monotonically increasing}] = 1$ according to the prior and let $uUB_\alpha(x) := \inf\{y \in \mathbb{R} : \mathbb{P}[f(x) \leq y | D^{\text{train}}] \geq \alpha\} \forall x \in X$ be the α -credible upper bound (i.e., the α -quantile of the posterior distribution of $f(x)$).¹² Then it holds that $uUB_\alpha(x)$ is monotonically increasing (i.e., $x \leq \tilde{x} \implies uUB_\alpha(x) \leq uUB_\alpha(\tilde{x})$).*

Proof. Let $x \leq \tilde{x}$. For a shorter notation we write “ f is (M)” instead of “ f is monotonically increasing” and we define $\tilde{\mathcal{V}} := \{f \in Y^X : f \text{ is (M)}\}$. Then, from the definition of

¹¹Within this paper “monotonically increasing” should always be interpreted as “monotonically non-decreasing”.

¹²In the literature, $\mathbb{P}[f(x) \leq y | D^{\text{train}}, x]$ is often used instead of $\mathbb{P}[f(x) \leq y | D^{\text{train}}]$ which is equal for every given $x \in X$. In both notations, f is seen as a random variable in function space.

monotonicity, it follows for every $y \in \mathbb{R}$ that¹³

$$\begin{aligned} \{f : f(x) > y, f \text{ is (M)}\} &\subseteq \{f : f(\tilde{x}) > y, f \text{ is (M)}\} \\ \iff \{f : f(x) > y\} \setminus \tilde{\mathcal{V}}^c &\subseteq \{f : f(\tilde{x}) > y\} \setminus \tilde{\mathcal{V}}^c \\ \iff \mathbb{P}[\{f : f(x) > y\} | D^{\text{train}}] &\leq \mathbb{P}[\{f : f(\tilde{x}) > y\} | D^{\text{train}}] \\ \iff \mathbb{P}[\{f : f(x) \leq y\} | D^{\text{train}}] &\geq \mathbb{P}[\{f : f(\tilde{x}) \leq y\} | D^{\text{train}}] \end{aligned}$$

Since $uUB_\alpha(x)$ is the infimum, we know that for every $y < uUB_\alpha(x)$:

$$\mathbb{P}[\{f : f(\tilde{x}) \leq y\} | D^{\text{train}}] \leq \mathbb{P}[\{f : f(x) \leq y\} | D^{\text{train}}] < \alpha.$$

This means that every $y < uUB_\alpha(x)$ is too small to be equal to $uUB_\alpha(\tilde{x})$, thus $uUB_\alpha(x) \leq uUB_\alpha(\tilde{x})$. \square

Proposition 2. *Let \mathcal{H} be a hypothesis class that only contains monotonically increasing functions and let $uUB_{\mathcal{H}}(x) := \sup\{f(x) : f \in \mathcal{H}_D^{\text{train}}\}$ be an uUB, then $uUB_{\mathcal{H}}$ is monotonically increasing (i.e., $x \leq \tilde{x} \implies uUB_{\mathcal{H}}(x) \leq uUB_{\mathcal{H}}(\tilde{x})$).*

Proof. Let $x \leq \tilde{x}$, then $\sup\{f(x) : f \in \mathcal{H}_D^{\text{train}}\} \leq \sup\{f(\tilde{x}) : f \in \mathcal{H}_D^{\text{train}}\}$, since $\forall f \in \mathcal{H}_D^{\text{train}} : f(x) \leq f(\tilde{x})$. \square

Monotone Value Functions Do Not Imply Monotone Uncertainty. However, the model uncertainty $\hat{\sigma}_f$ (defining the width of the UBs) is *not* monotonic at all. For already observed training input points there is zero model uncertainty while smaller unobserved input points can have much bigger model uncertainty.

If one would simply use the prior knowledge about the monotonicity to improve the mean prediction (by assuring its monotonicity) but then estimate the uUB by simply adding a standard (e.g., original NOMU or Gaussian processes) estimator for the (scaled) model uncertainty $c \cdot \hat{\sigma}_f$ to the mean prediction to obtain an uUB, one would obtain non-monotonic uUBs violating Propositions 1 and 2.

If one would simply use ensemble methods (Lakshminarayanan, Pritzel, and Blundell 2017; Gal and Ghahramani 2016) with MVNNs as ensemble members the uUBs obtained from the formula given in (Lakshminarayanan, Pritzel, and Blundell 2017; Gal and Ghahramani 2016) (re-stated in (Heiss et al. 2022) for the noiseless case) would also lead to non-monotonic uUBs violating Propositions 1 and 2. In theory, this problem could be circumvented by directly using a certain quantile of the ensembles as uUB instead of calculating uUBs based on empirical mean and variance of the ensemble. However, even the 100%-quantile of the ensemble (the point-wise maximum of the ensemble predictions) would often not sufficiently capture enough uncertainty, since Heiss et al. (2022, Remark B.5) empirically showed that the uncertainty of ensemble methods often needs to be scaled up by a very big factor to capture enough uncertainty. Moreover, Kuleshov, Fenner, and Ermon (2018) empirically showed that the uncertainty needs

¹³For the second equivalence we use that for every measurable set A , we obtain $\mathbb{P}[A] - 0 = \mathbb{P}[A] - \mathbb{P}[\mathcal{V}^c] \leq \mathbb{P}[A \setminus \mathcal{V}^c] \leq \mathbb{P}[A]$, thus $\mathbb{P}[A \setminus \mathcal{V}^c] = \mathbb{P}[A]$.

to be calibrated to achieve good results. To summarize, ensemble methods of monotonic functions have the problem that their calibration is limited or calibrating them results in non-monotonic uUBs. Note that the calibration method from [Kuleshov, Fenner, and Ermon \(2018\)](#) cannot solve this problem. Furthermore, in the ICA setting of this paper, optimizing the acquisition function (i.e., the ML-based WDP) based on the uUBs obtained from deep ensembles ([Lakshminarayanan, Pritzel, and Blundell 2017](#)) would be computationally too expensive.

However, for our proposed uUB $\mathcal{M}_i^{\text{uUB}}$ the uncertainty can be calibrated by varying π_{exp} without sacrificing monotonicity of the uUB. In the limit $\pi_{\text{exp}} \rightarrow 0$ one would just obtain the mean prediction and in the limit $\pi_{\text{exp}} \rightarrow \infty$ in relation to explicit and implicit regularization one would obtain the 100%-uUB as solution to our optimization problem.

Linear Skip Connections We have a hyper-parameter (that is part of our HPO) that decides whether we add a trainable linear connection directly from the input to the output for $\mathcal{M}_i^{\text{uUB}}$ and $\mathcal{M}_i^{\text{mean}}$ as formally defined in [Definition F.1](#).

No Connections Between the 2 Sub-architectures The architecture suggested in [Heiss et al. \(2022\)](#) contains connections from the mean-sub-architecture to the uncertainty-sub-architecture (the dashed lines in ([Heiss et al. 2022](#), Figure 2)). In our architecture (see [Figure 1](#)) we do not use such connections for two reasons:

1. Solving the WDP via the MILP given in [Theorem 2](#) is computationally much faster because we can completely ignore $\mathcal{M}_i^{\text{mean}}$ for the MILP formulation.
2. In the case of [Heiss et al. \(2022\)](#), without these connections, the uncertainty would be completely independent from the mean prediction (or from the labels y^{train}), prohibiting ([Heiss et al. 2022](#), Desiderata D4). However, our architecture directly outputs the uUB instead of the uncertainty $\hat{\sigma}_f$, thus $\mathcal{M}_i^{\text{uUB}}$ is automatically not independent from the labels $\hat{v}_i(x^{(l)})$.

D.3 ICA-based New NOMU Loss

Definition D.1 (Smooth L1 Loss). The smooth L1 loss $L_1^\beta : \mathbb{R} \times \mathbb{R} \rightarrow \mathbb{R}$ with threshold parameter $\beta \geq 0$ is defined as follows:

$$L_1^\beta(x, y) = \begin{cases} \frac{0.5}{\beta} \cdot (x - y)^2, & |x - y| \leq \beta \\ |x - y| - 0.5 \cdot \beta, & \text{otherwise.} \end{cases} \quad (32)$$

Definition D.2 (Exponential Linear Unit (ELU)). The ELU function $ELU : \mathbb{R} \rightarrow \mathbb{R}$ (with default parameter $\alpha = 1$) is defined as follows:

$$ELU(x) = \begin{cases} x, & x \geq 0 \\ 1 \cdot (\exp(x) - 1), & x < 0. \end{cases} \quad (33)$$

Definition D.3 (Detailed ICA-based New NOMU Loss). Let $\pi = (\pi_{\text{sqr}}, \pi_{\text{exp}}, c_{\text{exp}}, \bar{\pi}, \underline{\pi}) \in \mathbb{R}_+^5$ be a tuple of hyperparameters. For a training set D^{train} , L^π is defined as

$$L^\pi(\mathcal{M}_i^{\text{uUB}}) := \pi_{\text{sqr}} \sum_{l=1}^{n^{\text{train}}} L_1^\beta(\mathcal{M}_i^{\text{uUB}}(x^{(l)}), y^{(l)}) \quad (34a)$$

$$+ \pi_{\text{exp}} \int_{[0,1]^m} g(0.01 - c_{\text{exp}}(\min\{\mathcal{M}_i^{\text{uUB}}(x), \mathcal{M}_i^{100\%-\text{uUB}}(x)\} - \mathcal{M}_i^{\text{mean}}(x))) dx \quad (34b)$$

$$+ \pi_{\text{exp}} c_{\text{exp}} \bar{\pi} \int_{[0,1]^m} L_1^\beta((\mathcal{M}_i^{\text{uUB}}(x) - \mathcal{M}_i^{100\%-\text{uUB}}(x))^+) dx \quad (34c)$$

$$+ \pi_{\text{exp}} c_{\text{exp}} \underline{\pi} \int_{[0,1]^m} L_1^\beta((\mathcal{M}_i^{\text{mean}}(x) - \mathcal{M}_i^{\text{uUB}}(x))^+) dx \quad (34d)$$

$$+ \pi_{\text{sqr}} \sum_{l=1}^{n^{\text{train}}} 0.001 (\mathcal{M}_i^{\text{uUB}}(x^{(l)}) - y^{(l)})^+ + 0.5 L_1^\beta((\mathcal{M}_i^{\text{uUB}}(x^{(l)}) - y^{(l)})^+, 0) \quad (34e)$$

where L_1^β is the smooth L1-loss with threshold β (see [Definition D.1](#)), $(\cdot)^+$ the positive part, and $g := 1 + ELU$ is convex monotonically increasing with ELU being the exponential linear unit (ELU) (see [Definition D.2](#)).

Detailed interpretations of all five terms (including [\(34e\)](#) which was added to slightly improve the numerical stability) are as follows:

[\(34a\)](#) enforces that $\mathcal{M}_i^{\text{uUB}}$ fits through the training data.

[\(34b\)](#) pushes $\mathcal{M}_i^{\text{uUB}}$ up as long as it is below the 100%-uUB $\mathcal{M}_i^{100\%-\text{uUB}}$. This force gets weaker the further $\mathcal{M}_i^{\text{uUB}}$ is above the mean $\mathcal{M}_i^{\text{mean}}$ (especially if c_{exp} is large). π_{exp} controls the overall strength of [\(9b\)](#) and c_{exp} controls how fast this force increases when $\mathcal{M}_i^{\text{uUB}} \rightarrow \mathcal{M}_i^{\text{mean}}$. Thus, increasing π_{exp} increases the uUB and increasing c_{exp} increases the uUB in regions where it is close to the mean. Weakening [\(9b\)](#) (i.e., $\pi_{\text{exp}} c_{\text{exp}} \rightarrow 0$) leads $\mathcal{M}_i^{\text{uUB}} \approx \mathcal{M}_i^{\text{mean}}$. Strengthening [\(9b\)](#) by increasing $\pi_{\text{exp}} c_{\text{exp}}$ in relation to regularization¹⁴ leads $\mathcal{M}_i^{\text{uUB}} \approx \mathcal{M}_i^{100\%-\text{uUB}}$. In practice, we obtain reasonable approximations to $\alpha\%$ -uUB with $\alpha \in [50, 100]$ depending on the value of $\pi_{\text{exp}} c_{\text{exp}}$ in relation to regularization.

[\(34c\)](#) enforces that $\mathcal{M}_i^{\text{uUB}} \leq \mathcal{M}_i^{100\%-\text{uUB}}$. In theory, [\(9c\)](#) would be redundant in the limit $\pi_{\text{sqr}} \rightarrow \infty$, because $\mathcal{M}_i^{\text{uUB}} \in \mathcal{V}_{D^{\text{train}}}$. The strength of this term is determined by $\bar{\pi} \cdot (\pi_{\text{exp}} c_{\text{exp}})$, where $\bar{\pi}$ is the [\(9c\)](#)-specific hyperparameter and $\pi_{\text{exp}} c_{\text{exp}}$ adjusts the strength of [\(9c\)](#) to [\(9b\)](#).

[\(34d\)](#) enforces $\mathcal{M}_i^{\text{uUB}} \geq \mathcal{M}_i^{\text{mean}}$. In theory, one should take the limit $\underline{\pi} \rightarrow \infty$. However, in practice, a moderate value of $\underline{\pi}$ is numerically more stable and typically enforces that $\mathcal{M}_i^{\text{uUB}} \geq \mathcal{M}_i^{\text{mean}}$. The interpretation of $\underline{\pi}$ and $\pi_{\text{exp}} c_{\text{exp}}$ is analogous to [\(9c\)](#).

[\(34e\)](#) is an asymmetric version of [\(34a\)](#) for numerical stability. Since [\(34b\)](#) pushes $\mathcal{M}_i^{\text{uUB}}$ for all $x \in \mathcal{X}$ upwards, $\mathcal{M}_i^{\text{uUB}}$ would have a tendency to give slightly too high predictions for training data points, but [\(34e\)](#) compensates this effect for slightly improved numerical stability. In theory [\(34e\)](#) would be redundant in the limit $\pi_{\text{sqr}} \rightarrow \infty$.

¹⁴Regularization can be early stopping or a small number of neurons (implicit) or L2-regularization on the parameters (explicit). The same principle would also hold true if one uses other forms of regularization such as L1-regularization or dropout.

As in (Heiss et al. 2022), in the implementation of L^π , we approximate Equations (34b) to (34d) (in the main paper Equations (9b) to (9d)) via MC-integration using additional, *artificial input points* $D^{\text{art}} := \{x^{(l)}\}_{l=1}^{n^{\text{art}}}$ $\overset{i.i.d.}{\sim} \text{Unif}([0, 1]^m)$, where we sample new artificial input points for each batch of our mini-batch gradient descent based training algorithm.

Furthermore, note that in practice we train $\mathcal{M}_i^{\text{mean}}$ and $\mathcal{M}_i^{\text{uUB}}$ simultaneously but where $\mathcal{M}_i^{\text{mean}}$ is *detached* (using `torch.tensor.detach()`) in the loss L^π such that L^π does not influence the mean MVNN $\mathcal{M}_i^{\text{mean}}$.

E Parameter Initialization for MVNNs

In this section, we provide more details on our new parameter initialization method for MVNNs (see Section 3.2). Specifically, we give recommendations on how to set the hyperparameters of our proposed i.i.d. mixture distribution depending on the architecture size of the considered MVNN.

E.1 Theoretical Results

Definition E.1 (Mixture Distribution). *We define the probability density g_{A_k, B_k, p_k} of an initial weight $W_{j,l}^{i,k}$ corresponding to an MVNN as¹⁵*

$$g_{A_k, B_k, p_k}(w) = \frac{1-p_k}{A_k} \mathbb{1}_{[0, A_k]}(w) + \frac{p_k}{B_k} \mathbb{1}_{[0, B_k]}(w), \quad (35)$$

which corresponds to a mixture distribution of $\text{Unif}[0, A_k]$ and $\text{Unif}[0, B_k]$.

We assume that each $W_{j,l}^{i,k}$ in the k -th layer is distributed according to Definition E.1. Then we obtain

$$\mu_k = \mathbb{E} \left[W_{j,l}^{i,k} \right] = (1-p_k) \frac{A_k}{2} + p_k \frac{B_k}{2}. \quad (36)$$

Moreover, by using that the variance of an $\text{Unif}[0, c]$ -distributed random variable is $\frac{c^2}{12}$ we get that

$$\sigma_k^2 = \mathbb{V} \left[W_{j,l}^{i,k} \right] = (1-p_k) \frac{A_k^2}{3} + p_k \frac{B_k^2}{3} - \mu_k^2. \quad (37)$$

In the following, we provide a rule how to set for each layer k , A_k , B_k and p_k depending on the dimension $d^{i,k-1}$ of the previous $(k-1)^{\text{st}}$ layer.

This rule ensures that the conditional expectation and the conditional variance are equal to two constants \mathbb{E}^{init} , and \mathbb{V}^{init} , which are independent of the dimension of the previous layer $d^{i,k-1}$. More formally, let $z^{i,k-1} \in \mathbb{R}^{d^{i,k-1}}$ be the output of the neurons in the $(k-1)^{\text{st}}$ layer, then we set

¹⁵The bidder index i is not relevant in this section and we assume that each bidder i has the same architecture. If bidders would have different layer widths $d^{i,k-1}$, then all the values $A_k, B_k, p_k, \mu_k, \sigma_k$ would depend on the bidder index i too, i.e., $A_{i,k}, B_{i,k}, p_{i,k}, \mu_{i,k}, \sigma_{i,k}$.

A_k, B_k and p_k such that¹⁶

$$\mathbb{E} \left[\left(W^{i,k} z^{i,k-1} \right)_j + b_j^{i,k} \middle| z^{i,k-1} = (1, \dots, 1)^\top \right] = \mathbb{E}^{\text{init}} \quad (38a)$$

$$\mathbb{V} \left[\left(W^{i,k} z^{i,k-1} \right)_j \middle| z^{i,k-1} = (1, \dots, 1)^\top \right] = \mathbb{V}^{\text{init}}. \quad (38b)$$

Remark E.1. *Equivalent formulations of (38a) are*

$$\begin{aligned} (38a) &\Leftrightarrow \mathbb{E} \left[\left(W^{i,k} (1, \dots, 1)^\top \right)_j + b_j^{i,k} \right] = \mathbb{E}^{\text{init}} \\ &\Leftrightarrow \mathbb{E} \left[\left(W^{i,k} z^{i,k-1} \right)_j + b_j^{i,k} \middle| \overline{z^{i,k-1}} = 1 \right] = \mathbb{E}^{\text{init}}, \end{aligned}$$

where $\overline{z^{i,k-1}} = \frac{1}{d^{i,k-1}} \sum_{l=1}^{d^{i,k-1}} z_l^{i,k-1}$. And equivalent formulations of (38b) are

$$\begin{aligned} (38b) &\Leftrightarrow \mathbb{V} \left[\left(W^{i,k} (1, \dots, 1)^\top \right)_j \right] = \mathbb{V}^{\text{init}} \\ &\Leftrightarrow \mathbb{V} \left[\left(W^{i,k} z^{i,k-1} \right)_j \middle| z^{i,k-1} \right] = \mathbb{V}^{\text{init}} \left(\overline{z^{i,k-1}} \right)^2, \end{aligned}$$

where $\overline{z^{i,k-1}}^2 = \frac{1}{d^{i,k-1}} \sum_{l=1}^{d^{i,k-1}} \left(z_l^{i,k-1} \right)^2$.

The solution to problem (38) is not unique, but we propose three hyperparameters $B^{\text{init}}, b^{\text{init}}, \epsilon \in \mathbb{R}_+$ to characterize one specific solution that has multiple nice properties (see Theorem 3).

Definition E.2 (Scaling Rule). *For any choice of hyperparameters $\mathbb{E}^{\text{init}}, \mathbb{V}^{\text{init}}, B^{\text{init}}, b^{\text{init}}, \epsilon \in \mathbb{R}_+$ we propose the following values for B_k, A_k and p_k (for a shorter notation we write d instead of $d^{i,k-1} \in \mathbb{N}_+$):*

$$B_k = \begin{cases} \max \left(\frac{3\mathcal{M}_k^2 + 3d\mathbb{V}^{\text{init}}}{2\mathcal{M}_k d} + \frac{\epsilon}{d}, B^{\text{init}} \right) & , d > \frac{\mathcal{M}_k^2}{3\mathbb{V}^{\text{init}}} \\ \frac{d}{2} \mathcal{M}_k & , \text{else} \end{cases} \quad (39)$$

$$p_k = \begin{cases} 1 - \frac{B_k d^2 - 4B_k \mathcal{M}_k d + 4\mathcal{M}_k^2}{B_k^2 d^2 - 4B_k \mathcal{M}_k d + 3\mathcal{M}_k^2 + 3d\mathbb{V}^{\text{init}}} & , d > \frac{\mathcal{M}_k^2}{3\mathbb{V}^{\text{init}}} \\ 1 & , \text{else} \end{cases} \quad (40)$$

$$A_k = \begin{cases} \frac{2\mathcal{M}_k - B_k d p_k}{d(1-p_k)} & , d > \frac{\mathcal{M}_k^2}{3\mathbb{V}^{\text{init}}} \\ 0 & , \text{else}, \end{cases} \quad (41)$$

$$W_{j,l}^{i,k} \overset{i.i.d.}{\sim} g_{A_k, B_k, p_k} \quad (42)$$

$$b_j^{i,k} \overset{i.i.d.}{\sim} \text{Unif}[-b^{\text{init}}, 0] \quad (43)$$

where $\mathcal{M}_k = \mathbb{E}^{\text{init}} + \frac{b^{\text{init}}}{2}$ and where g_{A_k, B_k, p_k} is the mixture distribution described in Definition E.1 and where all weights and biases are sampled independently.

Finally, when using the scaling rule from Definition E.2, we can prove the following theorem.

Theorem 3. *For any choice of hyperparameters $\mathbb{E}^{\text{init}}, \mathbb{V}^{\text{init}}, B^{\text{init}}, b^{\text{init}}, \epsilon \in \mathbb{R}_+$, for every $k \in \{1, \dots, K_i\}$,*

¹⁶Note that $\mathbb{E}^{\text{init}} = (38a)$ (`init_E` in our code) includes already the bias, while $\mathbb{V}^{\text{init}} = (38b)$ (`init_V` in our code) does not include the bias. But this is a simple additive term that could easily be adjusted. One could easily include the bias in both or in none of them to make it more consistent.

for every dimension $d^{i,k-1} \in \mathbb{N}_+$ it holds that if we sample according to the distribution described in Definition E.2, we obtain that:¹⁷

1. (38a) holds,
2. $\mathbb{V} \left[(W^{i,k} z^{i,k-1})_j \middle| z^{i,k-1} = (1, \dots, 1)^\top \right] \geq \mathbb{V}^{\text{init}}$ holds,
3. (38b) holds if $d^{i,k-1} > \frac{\mathcal{M}_k^2}{3\mathbb{V}^{\text{init}}}$,
4. $\mathbb{P} \left[W_{j,l}^{i,k} = 0 \right] = 0$ if $\epsilon > 0$,
5. $\mathbb{P} \left[W_{j,l}^{i,k} = 0 \right] = 1 - p_k$ if $\epsilon = 0$ and $B^{\text{init}} < B_k$,
6. $\mathbb{P} \left[W_{j,l}^{i,k} < 0 \right] = 0$,
7. $\mathbb{P} \left[W_{j,l}^{i,k} > B_k \right] = 0$,
8. $B_k \geq \frac{3\mathbb{V}^{\text{init}}}{2\mathcal{M}_k}$,
9. $\lim_{d^{i,k-1} \rightarrow \infty} B_k = \max \left\{ \frac{3\mathbb{V}^{\text{init}}}{2\mathcal{M}_k}, B^{\text{init}} \right\}$.

Proof. First, note that¹⁸

$$\begin{aligned}
(38a) &\Leftrightarrow \mathbb{E} \left[(W^{i,k} z^{i,k-1})_j + b_j^{i,k} \middle| z^{i,k-1} = 1 \right] = \mathbb{E}^{\text{init}} \\
&\Leftrightarrow \mathbb{E} \left[(W^{i,k} z^{i,k-1})_j \middle| z^{i,k-1} = 1 \right] = \mathbb{E}^{\text{init}} - \mathbb{E} \left[b_j^{i,k} \right] \\
&\Leftrightarrow d^{i,k-1} \mathbb{E} \left[W_{j,l}^{i,k} \right] = \mathbb{E}^{\text{init}} + \frac{b^{\text{init}}}{2} \\
&\Leftrightarrow \mathbb{E} \left[W_{j,l}^{i,k} \right] = \frac{\mathcal{M}_k}{d^{i,k-1}}.
\end{aligned}$$

We prove this in section ‘‘Proof of item 1’’ of the **MATHEMATICA SCRIPT**¹⁹, where we use the notation $d := d^{i,k-1}$, $M := \mathcal{M}_k$, $V := \mathbb{V}^{\text{init}}$, $\epsilon := \epsilon$, $B^{\text{init}} := B^{\text{init}}$, $B_{\text{choice}} := B_k$ given in (39), $p_{\text{choice}} := p_k$ given in (40), $A_{\text{choice}} := A_k$ given in (41) and $\mathbb{E} \text{ of } W := \mathbb{E} \left[W_{j,l}^{i,k} \right]$ computed in (36). This proves item 1.

¹⁷We assume that \mathbb{E}^{init} , \mathbb{V}^{init} and d are strictly positive. However, B^{init} , b^{init} and ϵ could in theory also be set to 0 and Theorem 3 is formulated such that it would still hold true for $B^{\text{init}}, b^{\text{init}}, \epsilon \in \mathbb{R}_+ \cup \{0\}$.

¹⁸For this calculation we use the seemingly more general formulation from Remark E.1, so that one can also see the proof of the part regarding (38a) in Remark E.1.

¹⁹You can open the **MATHEMATICA SCRIPT** including the results in your web-browser (https://www.wolframcloud.com/obj/jakob.heiss/Published/MVNN_initialization_V1.4.nb) without the need to install anything on your computer. (The interactive plot might only work if you open the script with an installed version of Mathematica, but it is not necessary for the proof.) We use a computer algebra system to make it much more convenient to check the correctness of our proof. Some of the terms that appear in this proof are already very long as one can see for example in section ‘‘Proof of item 2 and 3’’ in our **MATHEMATICA SCRIPT**. Simplifying these terms by hand would take multiple pages of very tedious calculations, which would be highly prone to typos and other mistakes. Within our **MATHEMATICA SCRIPT** we only use exact symbolic methods and no numerical approximations (except for the visualizations).

We manipulate

$$\begin{aligned}
(38b) &\Leftrightarrow \mathbb{V} \left[(W^{i,k} z^{i,k-1})_j \middle| z^{i,k-1} = (1, \dots, 1)^\top \right] = \mathbb{V}^{\text{init}} \\
&\Leftrightarrow d^{i,k-1} \mathbb{V} \left[W_{j,l}^{i,k} \right] = \mathbb{V}^{\text{init}} \\
&\Leftrightarrow \mathbb{V} \left[W_{j,l}^{i,k} \right] = \frac{\mathbb{V}^{\text{init}}}{d^{i,k-1}}.
\end{aligned}$$

We prove this in section ‘‘Proof of item 2 and 3’’ of the **MATHEMATICA SCRIPT** with the additional notation $\mathbb{V} \text{ of } W := \mathbb{V} \left[W_{j,l}^{i,k} \right]$ computed in (37). This section proves items 2 and 3.

To show item 4 it is sufficient to show $A_k > 0$ (because of $A_k \leq B_k$, as shown in section ‘‘Proof of item 7: ($A \leq B$)’’ or ($p_k = 1$ and $B_k > 0$). If $d^{i,k-1} > \frac{\mathcal{M}_k^2}{3\mathbb{V}^{\text{init}}}$, we show $A_k > 0$ in section ‘‘Proof of item 4’’ of the **MATHEMATICA SCRIPT**. In the other case $p_k = 1$ and $B_k > 0$ as one can directly see from (39) and (40).

To show item 5, it is sufficient to show that $A_k = 0$. Section ‘‘Proof of item 5’’ of the **MATHEMATICA SCRIPT** shows in the case $d > \frac{\mathcal{M}_k^2}{3\mathbb{V}^{\text{init}}}$ that $A_k = 0 \iff (\epsilon = 0 \text{ and } B^{\text{init}} \leq \frac{3\mathcal{M}_k^2 + 3d\mathbb{V}^{\text{init}}}{2\mathcal{M}_k d})$. By definition this statement is equiv-

alent to $A_k = 0 \iff B_k = \frac{3\mathcal{M}_k^2 + 3d\mathbb{V}^{\text{init}}}{2\mathcal{M}_k d}$. Finally, since ($\epsilon = 0$ and $B^{\text{init}} < B_k$) $\implies B_k = \frac{3\mathcal{M}_k^2 + 3d\mathbb{V}^{\text{init}}}{2\mathcal{M}_k d}$, item 5 holds true. In the case $d^{i,k-1} \leq \frac{\mathcal{M}_k^2}{3\mathbb{V}^{\text{init}}}$, $A_k = 0$ (i.e., item 5) follows directly from (41). Note that $B_k > 0$ always holds true, since we always assume $\mathcal{M}_k > 0$ and $d > 0$.

Item 6 follows directly from Definition E.1 and the fact that $A_k \geq 0$ and $B_k \geq 0$ (see section ‘‘Proof of item 6’’ in the **MATHEMATICA SCRIPT**).

Item 7 follows directly from Definition E.1 and $A_k \leq B_k$ (see section ‘‘Proof of item 7: ($A \leq B$)’’ in the **MATHEMATICA SCRIPT**).

Item 8 is shown for the two cases in section ‘‘Proof of item 8’’ of the **MATHEMATICA SCRIPT**.

Item 9 is shown in section ‘‘Proof of item 9’’ in our **MATHEMATICA SCRIPT**. \square

Discussion of Theorem 3. Items 1 and 3 in Theorem 3 tell us that our initialization scheme actually solves problem (38) if $d^{i,k-1} > \frac{\mathcal{M}_k^2}{3\mathbb{V}^{\text{init}}}$. Note that problem (38) does not have any solution for for $d^{i,k-1} \leq \frac{\mathcal{M}_k^2}{3\mathbb{V}^{\text{init}}}$ (as can be seen in the first 5 lines of our **MATHEMATICA SCRIPT** with the notation explained in the proof of Theorem 3). However, items 1 and 2 in Theorem 3 tell us that we still have a reasonable initialization scheme for $d^{i,k-1} \leq \frac{\mathcal{M}_k^2}{3\mathbb{V}^{\text{init}}}$ that solves the relaxed problem of items 1 and 2. In practice solutions to this relaxed problem are still fine, since it also prevents us from exploding expectation or vanishing variance. Too much variance in the initialization is less of a problem.²⁰

²⁰Alternatively one could consider to relax problem (38) in the other direction by allowing smaller expectation instead of bigger variance, which would also be fine in practice. A solution to this alternative relaxed problem could be simply achieved by changing the definition of B_k in the ‘‘else’’-case of (39).

Items 4 and 5 motivate to choose $\epsilon > 0$ to prevent weights being initialized to zero, which can lead to bad local minima.

Item 6 guarantees that our network is actually a valid MVNN at initialization fulfilling the non-negativity constraints of the weights at initialization.²¹

Items 7 to 9 give us guarantees on the upper bound of the weights.

E.2 Recommended Hyperparameter Choices

In this section, we provide intuition about each hyperparameter $\mathbb{E}^{\text{init}}, \mathbb{V}^{\text{init}}, B^{\text{init}}, b^{\text{init}}, \epsilon \in \mathbb{R}_+$ and recommendations on how to set them in practice.

1. **Parameter \mathbb{E}^{init} :** (`init_E` in our code) gives the conditional expectation (38a) of a pre-activated neuron (including bias) conditioned on $z^{i,k-1} = 1$ (see item 1 in Theorem 3 and Remark E.1). This corresponds to an upper bound of the expected value of the MVNN $\mathbb{E}[\mathcal{M}_i^\theta((1, \dots, 1))]$ (i.e., the predicted value of the full bundle) at initialization of the network, if all cutoffs $t^{i,k}$ of the bReLU activation function are equal to 1. \mathbb{E}^{init} is approximately equal to $\mathbb{E}[\mathcal{M}_i^\theta((1, \dots, 1))]$ if $\mathbb{E}^{\text{init}} \geq 1$.

If you normalize the data such that the full bundle has always value 1 (i.e., $\hat{v}_i((1, \dots, 1)) = 1$), setting $\mathbb{E}^{\text{init}} = 1$ is our recommended choice. If you choose to initialize the bReLU cutoffs $t^{i,k}$ i.i.d. uniformly at random, i.e., $t^{i,k} \sim \text{Unif}(0, 1)$, then $\mathbb{E}^{\text{init}} \in [1, 2]$ is recommended, because in this case $\frac{\mathbb{E}^{\text{init}}}{2}$ is an upper bound for the expectation of the pre-activated values²² $o_j^{i,k}$ of any neuron in the MVNN at initialization for $k > 1$. This can be seen as follows:

$$\mathbb{E}[o_j^{i,k}] \stackrel{\text{Remark E.1}}{=} (\mathbb{E}^{\text{init}} - \mathbb{E}[b_j^{i,k}])\mathbb{E}[z_1^{i,k-1}] + \mathbb{E}[b_j^{i,k}] \quad (44)$$

$$\leq (\mathbb{E}^{\text{init}} - \mathbb{E}[b_j^{i,k}])\mathbb{E}[t^{i,k-1}] + \mathbb{E}[b_j^{i,k}] \quad (45)$$

$$= \frac{\mathbb{E}^{\text{init}} + \frac{b^{\text{init}}}{2}}{2} - \frac{b^{\text{init}}}{2} \quad (46)$$

$$= \frac{\mathbb{E}^{\text{init}}}{2} - \frac{b^{\text{init}}}{4} < \frac{\mathbb{E}^{\text{init}}}{2}, \quad (47)$$

where the second inequality follows from the definition of the bRelu activation function. Specifically, this also shows for $j = 1$ and $k = K_i$ that $\frac{\mathbb{E}^{\text{init}}}{2}$ is an upper bound

²¹Note that if we would initialize our network with a weight-distribution that solves problem (38), but does not fulfill Item 6 (e.g. a generic initialization with $\mu_k = 0$ and $\sigma_k \propto \frac{1}{\sqrt{d^{i,k-1}}}$), we would get a valid MVNN after the first gradient step, which projects all the negative weights to zero. However, this almost initial network would have exploding conditional expectations, i.e., almost all neurons would have pre-activations $o_j^{i,k} > 1$ independent of the input training data point and thus one would end up with an almost constant function and zero gradients as shown in Figure 5.

²²Recall, that $o_j^{i,k}$ is the pre-activated value of the j -th neuron in the k -th layer (of the i -th bidder) including biases.

for $\mathbb{E}[\mathcal{M}_i^\theta((1, \dots, 1))] = o_1^{i,K_i}((1, \dots, 1))$ at initialization.²³ If the values of your MVNN are in a different order of magnitude, you should scale your data in a pre-processing step to $[0, 1]$.

2. **Parameter \mathbb{V}^{init} :** (`init_V` in our code) gives the conditional variance (38b) of a pre-activated neuron (without bias) conditional on $z^{i,k-1} = (1, \dots, 1)^\top$, if $d^{i,k-1} > \frac{\mathcal{M}_k^2}{3\mathbb{V}^{\text{init}}}$ (see item 3 in Theorem 3). In any case, \mathbb{V}^{init} is a lower bound for this conditional variance (see item 2 in Theorem 3). Typically, we select $\mathbb{V}^{\text{init}} \in [1/50, 1]$. Choosing \mathbb{V}^{init} too small yields an almost deterministic network initialization. Since we prefer initial weights that are smaller than one, \mathbb{V}^{init} should not be chosen too large (i.e., preferably $\frac{3\mathbb{V}^{\text{init}}}{2\mathcal{M}_k} \leq 1$ because of items 7 to 9 in Theorem 3).
3. **Parameter b^{init} :** (`init_bias` in our code²⁴) All the biases of the MVNN $b_j^{i,k}$ are sampled uniformly at random from $[-b^{\text{init}}, 0]$ as given in eq. (43). Setting $b^{\text{init}} = 0.05$ is our recommendation, although any other small values would be sufficient. We discourage zero to avoid numerical issues during training.
4. **Parameter B^{init} :** (`init_b` in our code²⁴) B^{init} gives a lower bound for B_k in the case of large number of neurons (see item 9 in Theorem 3 and eq. (39)). The "big" weights are sampled from $\text{Unif}(0, B_k)$, i.e., B_k is an upper bound for the weights (see item 7 in Theorem 3). Usually, we prefer B_k that are not unnecessary big, but too small B_k leads to almost vanishing A_k (in the case of $d > \frac{\mathcal{M}_k^2}{3\mathbb{V}^{\text{init}}}$).²⁵ Thus, setting $B^{\text{init}} = 0.05$ is our recommendation (but one could also use any other small value including zero).
5. **Parameter ϵ :** (`init_little_const` in our code) prevents weights from being initialized to zero, i.e., $\epsilon > 0$ guarantees that no initial weight will be *exactly* zero, see item 4 in Theorem 3. Conversely setting $\epsilon = 0$ leads weights to be zero with probability $(1 - p_k)$ (see item 5 in Theorem 3). If one chooses ϵ too large B_k can become too large (see eq. (39)). Thus, setting $\epsilon = 0.1$ is our rec-

²³On the other hand one could argue that one wants the conditional expectation of pre-activated neurons to be smaller because of the smaller cut-offs. However, note especially for small values of \mathbb{E}^{init} , the actual expectation $\mathbb{E}[\mathcal{M}_i^\theta((1, \dots, 1))]$ at initialization decreases with increasing depth of the network, since the upper bound can loose its tightness as depth increases especially for $\mathbb{E}^{\text{init}} < 1$.

²⁴Be careful, when translating the notation of our paper into the notation of our code. B_k is `b` in our code and the biases b are denoted by `bias` in our code. b^{init} does *not* translate to `init_b`.

²⁵Section "Proof of item 5" in the [MATHEMATICA SCRIPT](#) shows that $A_k = 0$ iff $\epsilon = 0$ and $B_k \leq \frac{3\mathcal{M}_k^2 + 3d\mathbb{V}^{\text{init}}}{2\mathcal{M}_k d}$. This statement is equivalent to $A_k = 0$ iff $B_k = \frac{3\mathcal{M}_k^2 + 3d\mathbb{V}^{\text{init}}}{2\mathcal{M}_k d}$, which is the minimal possible choice for $B_k \in [\frac{3\mathcal{M}_k^2 + 3d\mathbb{V}^{\text{init}}}{2\mathcal{M}_k d}, \infty)$. By continuity $B_k \approx \frac{3\mathcal{M}_k^2 + 3d\mathbb{V}^{\text{init}}}{2\mathcal{M}_k d} \implies A_k \approx 0$. Note that in the other case $d \leq \frac{\mathcal{M}_k^2}{3\mathbb{V}^{\text{init}}}$, $p_k = 1$ and thus A_k is irrelevant for the mixture distribution from Definition E.1.

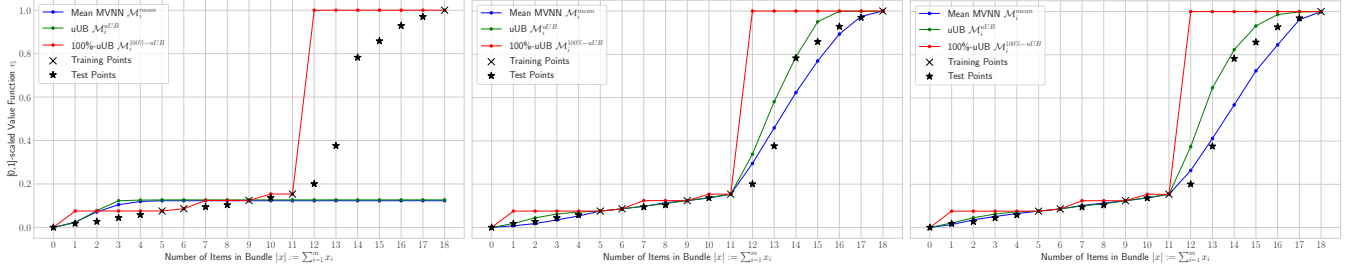


Figure 5: $\mathcal{M}_i^{\text{mean}}$, $\mathcal{M}_i^{\text{uUB}}$ and $\mathcal{M}_i^{100\text{-uUB}}$ along an increasing 1D subset-path in LSVM for the national bidder. **Left:** [64,64]-architecture with generic initialization fails. **Middle:** [64,64]-architecture with our initialization works. **Right:** even larger [256,256]-architecture with our initialization still works.

ommendation (similarly to b^{init} any other small value is also admissible).

In the last section of our **MATHEMATICA SCRIPT** we provide an interactive plot that shows how $B_k, A_k, p_k, \mathbb{V} \left[o_j^{i,k} - b_j^{i,k} \mid z^{i,k-1} = (1, \dots, 1)^\top \right]$ and $\mathbb{E} \left[o_j^{i,k} \mid z^{i,k-1} = (1, \dots, 1)^\top \right]$ depend on $d^{i,k-1}$ for different choices of our hyperparameters.

E.3 Visualization for Wider MVNNs

In this section, we provide an additional visualization for a wider MVNN that uses our proposed new initialization method.

In Figure 5 we present the results. Figure 5 confirms that our initialization method also properly works for an even larger MVNN-architecture with two hidden layers with 256 neurons per hidden layer. While the problems of the generic initialization methods described in Section 3.2 increase as the number of neurons increase, our initialization method can deal with an arbitrarily large number of neurons.

F MILP

In this section we provide more details on Section 3.3.

F.1 Proof of Theorem 2

In this section, we provide the proof of Theorem 2.

First, we show in Lemma 1 how to encode an arbitrary single hidden MVNN layer into multiple linear constraints. For this fix a bidder $i \in N$ and an arbitrary layer $k \in \{1, \dots, K_i - 1\}$. Recall, that $z^{i,k-1} \in \mathbb{R}^{d^{i,k-1}}$ denotes the output of the previous layer (with $z^{i,0}$ being equal to the input $x \in \mathbb{R}^{d^{i,0}} = \mathbb{R}^m$) and that $o^{i,k} := W^{i,k} z^{i,k-1} + b^{i,k}$ denotes the *pre-activated* output of the k^{th} layer with $l^{i,k} \leq o^{i,k} \leq u^{i,k}$, where the tight lower/upper bound $l^{i,k} / u^{i,k}$ can be computed by forward-propagating the empty/full bundle. Then the following Lemma holds:²⁶

²⁶All vector inequalities should be understood component-wise.

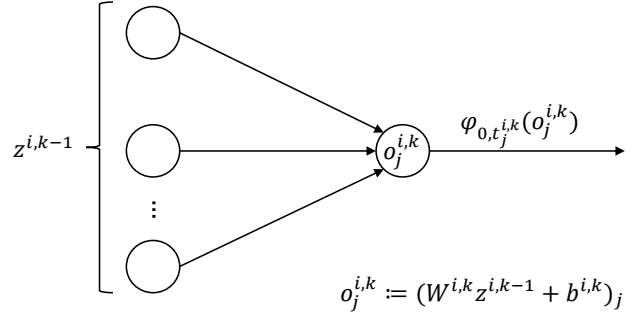


Figure 6: Schematic representation of the j^{th} neuron in the k^{th} layer. Shown are the output $z^{i,k-1}$ of the previous $(k-1)^{\text{st}}$ layer, the pre-activated output $o_j^{i,k}$ of the j^{th} neuron in the k^{th} layer, and the output of the j^{th} neuron of the k^{th} layer after applying bRELU $\varphi_{0,t_j^{i,k}}(o_j^{i,k}) = \min(t_j^{i,k}, \max(0, o_j^{i,k}))$.

Lemma 1. Consider the following set of linear constraints:

$$z^{i,k} \leq \alpha^{i,k} \cdot t^{i,k} \quad (48)$$

$$z^{i,k} \leq o^{i,k} - l^{i,k} \cdot (1 - \alpha^{i,k}) \quad (49)$$

$$z^{i,k} \geq \beta^{i,k} \cdot t^{i,k} \quad (50)$$

$$z^{i,k} \geq o^{i,k} + (t^{i,k} - u^{i,k}) \cdot \beta^{i,k} \quad (51)$$

$$\alpha^{i,k} \in \{0, 1\}^{d^{i,k}}, \beta^{i,k} \in \{0, 1\}^{d^{i,k}}. \quad (52)$$

Then it holds for the output of the k^{th} layer $\varphi_{0,t^{i,k}}(o^{i,k}) = z^{i,k}$.

Proof. Recall, that $o^{i,k} := W^{i,k} z^{i,k-1} + b^{i,k}$ denotes the pre-activated output of the k^{th} layer. Let $j \in \{1, \dots, d^{i,k}\}$ denote the j^{th} neuron of that layer and let $l_j^{i,k} \leq o_j^{i,k} \leq u_j^{i,k}$, where $l_j^{i,k}$ and $u_j^{i,k}$ are the tight box bounds computed by forward propagating the empty, i.e., $x = (0, \dots, 0)$, and the full, i.e., $x = (1, \dots, 1)$ bundle (see (Weissteiner et al. 2022a, Appendix C.5 and Fact C.1)). Moreover, let $\varphi_{0,t_j^{i,k}}(o_j^{i,k}) = \min(t_j^{i,k}, \max(0, o_j^{i,k}))$ with $t_j^{i,k} \geq 0$ be the output of the j^{th} neuron in the k^{th} layer. In Figure 6, we

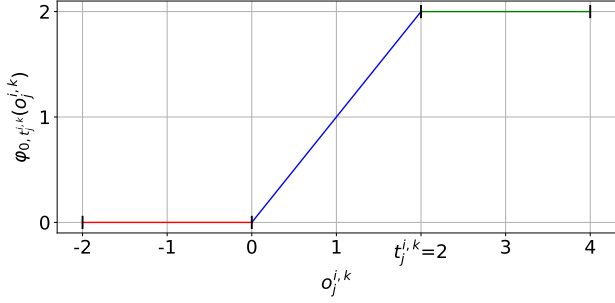


Figure 7: Example plot for agent i , layer k and neuron j of the bReLU activation function $\varphi_{0,t_j^{i,k}}(\cdot) := \min(t_j^{i,k}, \max(0, \cdot))$ (Weissteiner et al. 2022a) with cutoff $t_j^{i,k} = 2$ in the interval $[-2, 4]$. Shown are the pre-activated output $o_j^{i,k}$ of the j^{th} neuron in the k^{th} layer (x-axis) and the output of the j^{th} neuron in the k^{th} layer after applying bReLU (y-axis).

present a schematic representation for a single neuron. In Figure 7, we present an example of the bReLU activation function.

We distinguish the following three exclusive cases:

- **Case 1:** $o_j^{i,k} < 0$, i.e., the red line segment in Figure 7. Per definition it follows that $\varphi_{0,t_j^{i,k}}(o_j^{i,k}) = 0$. Setting $\alpha_j^{i,k} = \beta_j^{i,k} = 0$ in Equations (48) to (52) implies that $z_j^{i,k} = 0$.
- **Case 2:** $o_j^{i,k} \in [0, t_j^{i,k}]$, i.e., the blue line segment in Figure 7. Per definition it follows that $\varphi_{0,t_j^{i,k}}(o_j^{i,k}) = o_j^{i,k}$. Setting $\alpha_j^{i,k} = 1$ and $\beta_j^{i,k} = 0$ in Equations (48) to (52) implies that $z_j^{i,k} = o_j^{i,k}$.
- **Case 3:** $o_j^{i,k} > t_j^{i,k}$, i.e., the green line segment in Figure 7. Per definition it follows that $\varphi_{0,t_j^{i,k}}(o_j^{i,k}) = t_j^{i,k}$. Setting $\alpha_j^{i,k} = \beta_j^{i,k} = 1$ in Equations (48) to (52) implies that $z_j^{i,k} = t_j^{i,k}$.

Thus, in total $z_j^{i,k} = \varphi_{0,t_j^{i,k}}(o_j^{i,k})$. \square

Using Lemma 1, we can now proof Theorem 2 which provides our new and more succinct MILP formulation.

Proof. Consider the ML-based WDP from Equation (10). For each bidder $i \in N$, we first set $z^{i,0}$ equal to the input bundle a_i . Then we proceed by using Lemma 1 for $k = 1$, i.e., we reformulate the output of the 1st layer as the linear Equations (48) to (51). We iterate this procedure until we have reformulated the last hidden layer, i.e, layer $k = K_i - 1$. Doing so for each bidder $i \in N$ yields the desired MILP formulation from Theorem 2. \square

F.2 Removing Constraints via Box Bounds

Let $l_j^{i,k} \leq o_j^{i,k} \leq u_j^{i,k}$, where $l_j^{i,k}$ and $u_j^{i,k}$ are the *tight* box bounds computed by forward propagating the empty, i.e., $x = (0, \dots, 0)$, and the full, i.e., $x = (1, \dots, 1)$ bundle (see (Weissteiner et al. 2022a, Appendix C.5 and Fact C.1)).

In the following cases, one can remove the constraints and corresponding variables in Lemma 1 and thus also in Theorem 2.

- **Case 1:** $0 \leq t_j^{i,k} < l_j^{i,k} \leq u_j^{i,k}$. Then one can simply set

$$z_j^{i,k} := t_j^{i,k} \quad (53)$$

and remove the j^{th} components from Equations (48) to (52) of the corresponding layer k ($o_j^{i,k}$ lies for sure in the green line segment in Figure 7).

- **Case 2:** $l_j^{i,k} \leq u_j^{i,k} < 0 \leq t_j^{i,k}$. Then one can simply set

$$z_j^{i,k} := 0 \quad (54)$$

and remove the j^{th} components from Equations (48) to (52) of the corresponding layer k ($o_j^{i,k}$ lies for sure in the red line segment in Figure 7).

- **Case 3:** $0 \leq l_j^{i,k} \leq u_j^{i,k} \leq t_j^{i,k}$. Then one can simply set

$$z_j^{i,k} := o_j^{i,k} \quad (55)$$

and remove the j^{th} components from Equations (48) to (52) of the corresponding layer k ($o_j^{i,k}$ lies for sure in the blue line segment in Figure 7).

- **Case 4:** $0 \leq l_j^{i,k} \leq t_j^{i,k} < u_j^{i,k}$. Then one can set

$$\alpha_j^{i,k} := 1 \quad (56)$$

and only one binary decision variable for the j^{th} neuron of the k^{th} layer remains. ($o_j^{i,k}$ lies for sure in the union of the blue and green line segment in Figure 7).

- **Case 5:** $l_j^{i,k} \leq 0 < u_j^{i,k} \leq t_j^{i,k}$. Then one can set

$$\beta_j^{i,k} := 0 \quad (57)$$

and only one binary decision variable for the j^{th} neuron of the k^{th} layer remains. ($o_j^{i,k}$ lies for sure in the union of the red and blue line segment in Figure 7).

F.3 MILP for MVNNs with Linear Skip Connection

In this section, we provide a simple extension of the MILP in Theorem 2 for MVNNs with a linear skip connection. First, we define MVNNs with a linear skip connection.

Definition F.1 (MVNN with Linear Skip Connection). *An MVNN with linear skip connection $\mathcal{M}_i^{\text{lskip},\theta} : \mathcal{X} \rightarrow \mathbb{R}_+$ for agent $i \in N$ is defined as*

$$\begin{aligned} \mathcal{M}_i^{\text{lskip},\theta}(x) = & W^{i,K_i} \varphi_{0,t^{i,K_i}}(\dots \varphi_{0,t^{i,1}}(W^{i,1}x + b^{i,1}) \dots) \\ & + W^{i,0}x, \end{aligned} \quad (58)$$

- $K_i + 1 \in \mathbb{N}$ is the number of layers ($K_i - 1$ hidden layers),
- $\{\varphi_{0,t^{i,k}}\}_{k=1}^{K_i-1}$ are the MVNN-specific activation functions with cutoff $t^{i,k} > 0$, called bounded ReLU (bReLU):

$$\varphi_{0,t^{i,k}}(\cdot) := \min(t^{i,k}, \max(0, \cdot)) \quad (59)$$

- $W^i := (W^{i,k})_{k=0}^{K_i}$ with $W^{i,k} \geq 0$ and $b^i := (b^{i,k})_{k=1}^{K_i-1}$ with $b^{i,k} \leq 0$ are the non-negative weights and non-positive biases of dimensions $d^{i,k} \times d^{i,k-1}$ (except $W^{i,0}$ which is of dimension $d^{i,K_i} \times d^{i,0}$) and $d^{i,k}$, whose parameters are stored in $\theta = (W^i, b^i)$, where $W^{i,0}$ represents the linear skip connection.

For the MILP of an MVNN with linear skip connection the only thing that changes is the objective, i.e., one needs to replace Equation (11) in Theorem 2 with

$$\max_{a \in \mathcal{F}, z^{i,k}, \alpha^{i,k}, \beta^{i,k}} \left\{ \sum_{i \in N} W^{i,K_i} z^{i,K_i-1} + W^{i,0} z^{i,0} \right\} \quad (60)$$

G Experiment Details

In this section, we present all details of our experiments from Section 4.

G.1 SATS domains

In this section, we provide a more detailed overview of the three SATS domains²⁷, which we use to experimentally evaluate BOCA:

- **Local Synergy Value Model (LSVM)** (Scheffel, Ziegler, and Bichler 2012) has 18 items, 5 *regional* and 1 *national bidder*. Complementarities arise from spatial proximity of items.
- **Single-Region Value Model (SRVM)** (Weiss, Lubin, and Seuken 2017) has 29 items and 7 bidders (categorized as *local*, *high frequency regional*, or *national*) and models large UK 4G spectrum auctions.
- **Multi-Region Value Model (MRVM)** (Weiss, Lubin, and Seuken 2017) has 98 items and 10 bidders (*local*, *regional*, or *national*) and models large Canadian 4G spectrum auctions.

In the efficiency experiments in this paper (i.e., Table 1, Table 3, Table 4, Table 5, and Table 6), we instantiated for each SATS domain the 50 synthetic CA instances with the seeds $\{10001, \dots, 10050\}$. We used **SATS version 0.8.0**. All experiments were conducted on a compute cluster running Debian GNU/Linux 10 with Intel Xeon E5-2650 v4 2.20GHz processors with 24 cores and 128GB RAM and Intel E5 v2 2.80GHz processors with 20 cores and 128GB RAM and Python 3.7.10.

G.2 Hyperparameter Optimization

In this section, we provide details on the exact hyperparameter ranges that we used in our HPO. Table 2 shows all hyperparameter ranges that we used. In the following, we explain selected hyperparameters:

²⁷We do not consider the simplest of all SATS domains, i.e., the *Global Synergy Value Model (GSVM)* (Goeree and Holt 2010), since prior work already achieves 0% efficiency loss without integrating any notion of uncertainty (Weissteiner et al. 2022a), and thus GSVM can be seen as already “solved”.

- **DROPOUT PROBABILITY DECAY FACTOR:** After each epoch t the dropout probability for the next epoch $t + 1$ p_{drop}^{t+1} is updated as: $p_{\text{drop}}^{t+1} = p_{\text{drop}}^t \cdot \kappa$, where κ denotes this factor.
- **CLIP GRAD NORM:** Parameter for gradient clipping in PYTORCH via `torch.nn.utils.clip_grad_norm_()`.
- **RANDOM INITIALIZED TS:** Uniform distribution, which is used to initialize the bReLU cutoffs $t^{i,k}$ i.i.d. uniformly at random, i.e. $t^{i,k} \sim \text{Unif}(A, B)$ (setting $A = B$ makes those cutoffs deterministic).
- **TRAINABLE TS:** If set to TRUE, the cutoffs of the bReLU activation function $\{t^{i,k}\}_{k=1}^{K_i-1}$ are learned (i.e., trained) during the training procedure of the corresponding MVNN.

Evaluation Metric HPO We motivate our choice of the two terms in our evaluation metric (18) in the following way:

1. The first term

$$|D^{\text{test}}|^{-1} \sum_{(x,y) \in D^{\text{test}}} \max\{(y - \mathcal{M}_i^{\text{uUB}}(x))q, (\mathcal{M}_i^{\text{uUB}}(x) - y)(1-q)\}$$

of (18) is the standard quantile-loss applied on the test data set. Achieving a low value in this evaluation metric is intuitively desirable since for values $q > 0.5$ we penalize predictions that are too low more severely than predictions that are too high. It is also theoretically well motivated, since the true²⁸ posterior q -credible bound $\text{uUB}_\alpha(x) := \inf\{y \in \mathbb{R} : \mathbb{P}[\hat{v}_i(x) \leq y | D^{\text{train}}] \geq \alpha\} \forall x \in X$ would minimize this evaluation metric in expectation. As we average this term over 100 different value functions and as we use a large test data set for each of them, this is a good approximation for the expectation.

2. The second term $\text{MAE}(D^{\text{train}})$ of (18) might appear to be counter-intuitive, because we are using the training data set. However, in BO it is particularly important to fit well through the noiseless training data points. First, the training data points in BO have already been chosen to lie in a region of potential maximizers. Second, in BO, relative uncertainty (Heiss et al. 2022, Appendix A.2.1.) and particularly Desiderata D2 from (Heiss et al. 2022) are more important than calibration as discussed in (Heiss et al. 2022, Appendix D.2.3). Adding a constant value to $\mathcal{M}_i^{\text{uUB}}$ would calibrate them but would not change the argmax (2) (i.e., would not change the selected queries). However, the 1st term of our evaluation metric (18) alone would assign quite low values to $\mathcal{M}_i^{\text{uUB}}$ of the form $\mathcal{M}_i^{\text{mean}} + c$. Fortunately, the second term $\text{MAE}(D^{\text{train}})$ prevents (18) from assigning low values to $\mathcal{M}_i^{\text{uUB}}$ of the form $\mathcal{M}_i^{\text{mean}} + c$.

G.3 Details MVNN-Training

Both for the HPO as well as when running our efficiency experiments, we use the following two techniques to achieve numerically more robust results.

²⁸By “true posterior” we denote the posterior coming from the “true prior” that we sample our value functions \hat{v}_i from.

CATEGORY	HYPERPARAMETER	RANGE	LOG-UNIFORM SAMPLING
DATA	NUMBER OF TRAINING DATA POINTS: $ D^{\text{TRAIN}} $	LSVM: 50 SRVM: 100 MRVM: 100	
	NUMBER OF TEST DATA POINTS: $ D^{\text{TEST}} $	LSVM: 2^{10} SRVM: 2^{13} MRVM: 2^{13}	
	NUMBER OF SATS INSTANCES	100	
GENERIC MVNN	ARCHITECTURE: (#NEURONS PER HIDDEN LAYER, #HIDDEN LAYERS)	LSVM: $\{(96, 1), (32, 2), (16, 3)\}$ SRVM: $\{(32, 2), (16, 3)\}$ MRVM: $\{(96, 1), (64, 1), (20, 2)\}$	
	LINEAR SKIP CONNECTION (SEE DEFINITION F.1)	{TRUE, FALSE}	
	BATCH SIZE	$\{ D^{\text{TRAIN}} /4, D^{\text{TRAIN}} /2, D^{\text{TRAIN}} \}$	
	EPOCHS	$\{4000 \frac{\text{BATCH SIZE}}{ D^{\text{TRAIN}} }, 4500 \frac{\text{BATCH SIZE}}{ D^{\text{TRAIN}} }, 5000 \frac{\text{BATCH SIZE}}{ D^{\text{TRAIN}} }, \dots, 8000 \frac{\text{BATCH SIZE}}{ D^{\text{TRAIN}} }\}$	
	DROPOUT PROBABILITY	[0, 0.8]	
	DROPOUT PROBABILITY DECAY FACTOR	[0.75, 1.0]	
GENERIC LOSS	OPTIMIZER	ADAM	
	LEARNING RATE	GSVM: [0.0002, 0.002] LSVM: [0.001, 0.01] SRVM: [0.0008, 0.006] MRVM: [0.0007, 0.004]	Yes
	L2-REGULARIZATION: λ (SEE EQUATION (9))	[1E-10, 1E-3]	Yes
	SMOOTH L1-LOSS β (SEE DEFINITION D.1)	{1/32, 1/64, 1/128}	
	CLIP GRAD NORM	[1E-6, 1]	Yes
	NEW NOMU LOSS	NUMBER OF ARTIFICIAL INPUT DATA POINTS: $ D^{\text{ART}} $ (SEE SECTION 3.1)	{64, 80, 96, ..., 512}
π_{SQR} (SEE EQUATION (9))		1	
π_{EXP} (SEE EQUATION (9))		[1E-6, 5E-1]	Yes
$\underline{\pi}$ (SEE EQUATION (9))		[64, 256]	Yes
$\overline{\pi}$ (SEE EQUATION (9))		0.25	
c_{EXP} (SEE EQUATION (9))		[64, 256]	Yes
MVNN INITIALIZATION	RANDOM INITIALIZED TS	UNIF(0,1)	
	TRAINABLE TS	{TRUE, FALSE}	
	INITIAL EXPECTATION: \mathbb{E}^{INIT} (SEE APPENDIX E.2)	[1, 2]	
	INITIAL VARIANCE: \mathbb{V}^{INIT} (SEE APPENDIX E.2)	[0.02, 0.16]	Yes
	INITIAL BIAS: b^{INIT} (SEE APPENDIX E.2)	0.05	
	INITIAL "B" CONSTANT: B^{INIT} (SEE APPENDIX E.2)	0.05	
	INITIAL "LITTLE" CONSTANT: ϵ (SEE APPENDIX E.2)	0.1	

Table 2: Hyperparameter ranges used in our HPO for random search. If not explicitly stated otherwise, the ranges apply to all considered SATS domains.

DOMAIN	QUANTILE PARAMETER Q	Q^{INIT}	Q^{ROUND}	Q^{MAX}	EFFICIENCY LOSS IN % \downarrow	REVENUE IN % \uparrow	RUNTIME IN HOURS
LSVM	0.60	40	4	100	0.69 ± 0.41	74.73 ± 3.68	4.90
	0.75	40	4	100	0.69 ± 0.44	75.07 ± 3.71	5.53
	0.90	40	4	100	0.39 ± 0.30	73.53 ± 3.72	15.64
	0.95	40	4	100	0.40 ± 0.35	73.88 ± 3.93	15.58
SRVM	0.60	40	4	100	0.16 ± 0.04	54.34 ± 1.48	24.67
	0.75	40	4	100	0.06 ± 0.02	54.22 ± 1.46	18.80
	0.90	40	4	100	0.54 ± 0.08	53.89 ± 1.44	33.90
	0.95	40	4	100	0.62 ± 0.11	54.25 ± 1.54	33.26
MRVM	0.60	40	4	100	7.88 ± 0.43	41.81 ± 1.06	61.48
	0.75	40	4	100	8.44 ± 0.43	41.89 ± 0.93	34.91
	0.90	40	4	100	7.77 ± 0.34	42.04 ± 0.89	28.15
	0.95	40	4	100	7.98 ± 0.34	42.28 ± 1.00	27.92

Table 3: Detailed BOCA results. We present efficiency loss, relative revenue and runtime with our MVNN-based uUB $\mathcal{M}_i^{\text{uUB}}$ as \mathcal{A}_i . Shown are averages including a 95%-normal-CI on a test set of 50 instances in all three considered SATS domains. The best MVNN-based uUBs per domain (w.r.t the quantile parameter q based on the lowest efficiency loss) are marked in grey.

1. At the end of the training procedure we use the best weights from all epochs, and not the ones from the last epoch.
2. If at the end of the training procedure the R^2 (coefficient of determination) was below 0.9 on the training set, we retrain once and finally select the model with the best performance across these two attempts.

G.4 Details MILP Parameters

In our experiments we use for all MILPs CPLEX version 20.1.0. . Furthermore, we set the following MILP parameters: `time_limit = 600 sec`, `relative_gap = 0.005`, `integrality_tol = 1e - 06`, `feasibility_tol = 1e - 09`. Thus, the MILP solver stops as soon as it has found a feasible integer solution proved to be within 0.5% of optimality and otherwise stops after 600 seconds. CPLEX is automatically proving upper bounds for the relative gap (using duality) while approximating the solution for the MILP. Thus, when CPLEX finds a solution with a relative gap of at most 0.5%, we have a guarantee that the solution found by CPLEX is *at most* 0.5% worse than the unknown true solution. However, we have no a priori theoretical guarantee that CPLEX is always able to find such a solution and such a bound within 600 sec. Note that we set the time limit to 600 sec to allow researchers with a limited budget to reproduce our results hundreds of times with different seeds, while achieving already SOTA. For an actual spectrum auction the additional costs for increasing the computational budget by a factor of 10 would be negligible compared to the statistical significant increase of 200 million USD of revenue gained from using BOCA instead of MVNN in the case of MRVM for example (see Appendix G.6). In our experiments, the median relative gaps²⁹ across all runs per domain in Table 1 were: LSVM=0.004987, SRVM=0.005000, MRVM=0.004991, indicating that in most of the runs the MILP solver found within the time limit an optimal solution within tolerance.

G.5 Details BOCA Results

In this section, we provide detailed efficiency loss results of BOCA. Specifically, we present in Table 3 efficiency loss results for all four HPO winner configurations (with respect to the evaluation metric based on the four different quantile parameters $q \in \{0.6, 0.75, 0.9, 0.95\}$). Furthermore, we present the *relative revenue* $\sum_{i \in N} p(R)_i / V(a^*)$ of an allocation $a_R^* \in \mathcal{F}$ and payments $p(R) \in \mathbb{R}_+^n$ determined by BOCA when eliciting reports R as well as the average runtime in hours for a single instance (i.e, how long it would take to run a single auction). Note that since we stop BOCA when we have already found an allocation with 0% efficiency loss, the relative revenue numbers (in LSVM and SRVM) are pessimistic and typically increase if we let BOCA run until Q^{\max} is reached. For the runtime results the opposite holds.

²⁹In CPLEX, the “relative gap” always refers to the proven upper bound of the relative gap.

G.6 Revenue

Comparing the revenue of BOCA (see Table 3) to the revenue of MVNN-MLCA and NN-MLCA in (Weissteiner et al. 2022a, Table 6), we see that overall the mean relative revenue is as good or better than SOTA. For LSVM (and SRVM) this comparison could be flawed because we stop computing further queries when reaching 0% efficiency loss as described above.

However, for MRVM, we always compute all 100 queries as can be seen in (Weissteiner et al. 2022a, Table 6). Thus MRVM allows for a fair comparison of the relative revenue. In MRVM, BOCA’s relative revenue is on average $\sim 7\%$ -points higher than the one of MVNN-MLCA. With a confidence of more than 95% the revenue of BOCA is by more than 4%-points (corresponding to ~ 200 million USD in this domain³⁰ (Ausubel and Baranov 2017)) better than the one of MVNN-MLCA. The comparison of BOCA to NN-MLCA is also in favour of BOCA, but much closer (and BOCA outperforms NN-MLCA in terms of social welfare with a $p_{\text{VAL}} = 2e-5$, see Table 1).

The strength of BOCA with respect to revenue is quite intuitive since each query that explores regions of high uncertainty in the bundle space is beneficial for all economies, while “exploiting” an allocation which leads to high efficiency in one certain economy is mainly beneficial for this certain economy (see Appendix A for the definition of main and marginal economies). As discussed in (Weissteiner et al. 2022a, Appendix E.3), MLCA queries the main economy more often than any other economy and revenue is high if the social welfare in the marginal economies is high relative to the social welfare in the main economy. Thus, exploration favours high revenue in settings (such as ours) where the main economy is queried more often than the marginal economies.

G.7 Understanding BOCA’s Performance Increase

In this section, we present further efficiency loss results when using only the mean MVNN $\mathcal{M}_i^{\text{mean}}$ of $\mathcal{M}_i^{\text{NOMU}}$ in MLCA as \mathcal{A}_i . We call this method OUR-MVNN-MLCA. Note that OUR-MVNN-MLCA does not integrate any explicit notion of uncertainty and is thus the same method as MVNN-MLCA from Weissteiner et al. (2022a), but now with our new proposed parameter initialization method (see Section 3.2) and optimized with our HPO. Thus, this experiment investigates how much of the performance gain is attributed to the integration of our notion of uncertainty compared to the other changes we made (i.e., our parameter initialization method and our HPO).

In Figure 8, we present the efficiency loss path plots for OUR-MVNN-MLCA (yellow) compared to the results presented in Figure 4 in the main paper. For each domain we

³⁰The revenue of the 2014 Canadian 4G auction was ~ 5 billion USD (Ausubel and Baranov 2017). Thus, 4%-points of 5 billion USD corresponds to ~ 200 million USD. If one accumulates the revenue of all spectrum auctions, one would obtain significantly larger values.

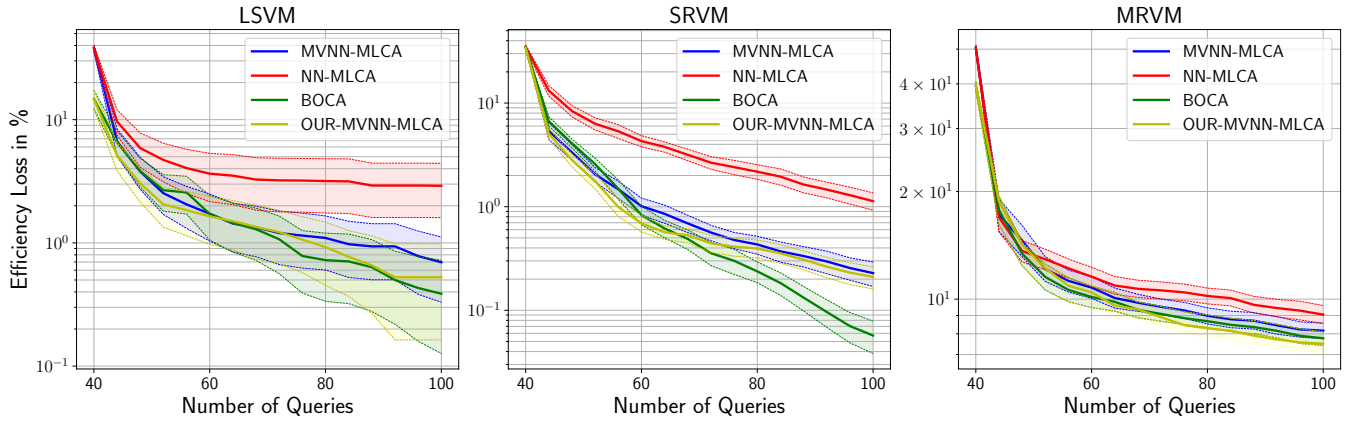


Figure 8: Efficiency loss paths (i.e., regret plots) for $Q^{\text{init}} = 40$ of OUR-MVNN-MLCA winners (yellow) from Table 4 compared to BOCA winners (green) from Table 3 and to the results presented in (Weissteiner et al. 2022a) of MVNNs (blue) and plain NNs (red). Shown are averages with 95% CIs over 50 instances.

DOMAIN	QUANTILE PARAMETER Q	Q^{INIT}	Q^{ROUND}	Q^{MAX}	EFFICIENCY LOSS IN % \downarrow	REVENUE IN % \uparrow	RUNTIME IN HOURS
LSVM	0.60	40	4	100	0.66 ± 0.44	74.93 ± 3.48	4.62
	0.75	40	4	100	0.61 ± 0.42	75.14 ± 3.53	4.16
	0.90	40	4	100	0.53 ± 0.41	73.80 ± 3.88	10.44
	0.95	40	4	100	0.56 ± 0.40	74.83 ± 3.67	10.31
SRVM	0.60	40	4	100	0.22 ± 0.04	54.24 ± 1.51	21.18
	0.75	40	4	100	0.21 ± 0.05	54.47 ± 1.51	17.81
	0.90	40	4	100	0.36 ± 0.06	54.51 ± 1.49	20.03
	0.95	40	4	100	0.35 ± 0.05	54.51 ± 1.48	19.14
MRVM	0.60	40	4	100	7.86 ± 0.42	41.91 ± 0.91	41.51
	0.75	40	4	100	8.41 ± 0.40	40.28 ± 0.92	6.89
	0.90	40	4	100	7.51 ± 0.47	40.22 ± 0.96	4.91
	0.95	40	4	100	8.01 ± 0.48	40.62 ± 1.08	9.03

Table 4: Detailed OUR-MVNN-MLCA results. We present efficiency loss, relative revenue and runtime of OUR-MVNN-MLCA, i.e., MLCA with our MVNN-based mean $\mathcal{M}_i^{\text{mean}}$ as \mathcal{A}_i . Shown are averages including a 95%-normal-CI on a test set of 50 instances in all three considered SATS domains. The best $\mathcal{M}_i^{\text{mean}}$ per domain (w.r.t the quantile parameter q) based on the lowest efficiency loss is marked in grey.

use for OUR-MVNN-MLCA (yellow) the best mean models $\mathcal{M}_i^{\text{mean}}$ from $\mathcal{M}_i^{\text{NOMU}}$ based on the smallest efficiency loss (i.e., the grey-marked winners from Table 4).

As expected, we see that BOCA, i.e., integrating a notion of uncertainty, is as good or better than OUR-MVNN-MLCA, i.e., only using the mean model. This effect is statistically significant in SRVM, while in LSVM and MRVM both lead to results that are statistically on par. The degree to which exploration via a notion of uncertainty is beneficial depends on intrinsic characteristics of the domain (e.g., the dimensionality or multi-modality of the objective function). Specifically, in MRVM where the query budget of $Q^{\text{max}} = 100$ is extremely small compared to the dimensionality of the domain (i.e., MRVM has $m = 98$ items and $n = 10$ bidders thus the dimensionality is $980 = 98 \cdot 10$), it appears that exploitation might be beneficial compared to adding exploration (De Ath et al. 2021) and the power of adding exploration may reveal itself only when increasing the query budget. However, in LSVM and SRVM ($m = 18$ and $m = 29$), we see that adding exploration with an uUB $\mathcal{M}_i^{\text{uUB}}$ decreases the efficiency loss. Finally, these results also suggest that our proposed new parameter initialization method for MVNNs discussed in Section 3.2 tends to be better than a simple generic one, i.e. OUR-MVNN-MLCA is in every domain on average better than MVNN-MLCA.

Finally, in Table 4 we present the complete results of this experiment for all quantile parameters q per domain.

We refer to Appendix G.8 for an additional comparison of BOCA and OUR-MVNN-MLCA for a reduced number of initial queries.

G.8 Reduced Number of Initial Queries

In this section, we present results of BOCA and OUR-MVNN-MLCA for a reduced number of initial random queries. Specifically, we chose $Q^{\text{init}} = 20$ initial random queries (instead of $Q^{\text{init}} = 40$ that were selected in the main set of experiments following prior work; see Table 3 and Table 4). All other parameters are left untouched.

Note that the previous literature used only $Q^{\text{init}} = 40$, since batching reduces the cost per queries in practice, i.e., not only the queries are costly but also the rounds are costly. Reducing Q^{init} from 40 to 20 increases the number of rounds from 15 to 20 (given that $Q^{\text{round}} = 4$ queries, i.e., 3 marginal economy queries and 1 main economy query, are asked per round). Furthermore, the experiments get computationally more costly as we reduce Q^{init} , because we need to perform more (MV)NN trainings and solve more MILPs.

Because of this, we only compare BOCA vs. OUR-MVNN-MLCA in this section (as in Appendix G.7). Thus, in this section, we do not study the benefits of our new initialization method (Section 3.2), and only focus on studying the benefits of incorporating our proposed uncertainty model (Section 3.1).

In Table 5 we present the BOCA results for $Q^{\text{init}} = 20$. To isolate the effect of the integrated uncertainty in BOCA, we present the corresponding results for OUR-MVNN-MLCA for $Q^{\text{init}} = 20$ in Table 6, (see Appendix G.7 for a description of this experiment setting).

Effect of Q^{init} Parameter Comparing Table 5 to Table 3, we see that by reducing the randomly sampled initial queries from $Q^{\text{init}} = 40$ to $Q^{\text{init}} = 20$, BOCA’s efficiency loss tends to be on average smaller for LSVM and MRVM and, perhaps surprisingly, larger for SRVM. However, by comparing the grey-marked winner models in each domain, we see that it does not make a statistically significant difference whether Q^{init} is chosen to be 20 or 40.

BOCA vs. OUR-MVNN-MLCA for $Q^{\text{init}} = 20$ Also when comparing BOCA to OUR-MVNN-MLCA for a reduced number of $Q^{\text{init}} = 20$ initial queries, i.e., comparing Table 5 to Table 6, we find that in each domain the BOCA winner model and the OUR-MVNN-MLCA winner model perform statistically on par (even though the average efficiency loss of the BOCA winner model is always better than that of the OUR-MVNN-MLCA winner model). This can also be seen in the efficiency loss paths (i.e., regret plots) shown in Figure 9. Furthermore, Figure 9 suggests that for a small query budget of $Q^{\text{max}} < 60$, exploitation might be more important, while for query budgets larger than 80, i.e., $Q^{\text{max}} > 80$, exploration might pay off more.

DOMAIN	QUANTILE PARAMETER Q	Q^{INIT}	Q^{ROUND}	Q^{MAX}	EFFICIENCY LOSS IN % \downarrow	REVENUE IN % \uparrow	RUNTIME IN HOURS
LSVM	0.60	20	4	100	0.79 ± 0.47	73.74 ± 3.65	5.93
	0.75	20	4	100	0.61 ± 0.42	73.99 ± 3.56	7.31
	0.90	20	4	100	0.37 ± 0.24	73.18 ± 3.60	23.99
	0.95	20	4	100	0.16 ± 0.20	72.84 ± 3.45	22.21
SRVM	0.60	20	4	100	0.14 ± 0.04	53.86 ± 1.44	32.07
	0.75	20	4	100	0.12 ± 0.09	53.87 ± 1.55	25.89
	0.90	20	4	100	0.72 ± 0.11	53.94 ± 1.59	45.20
	0.95	20	4	100	0.75 ± 0.11	54.09 ± 1.55	45.09
MRVM	0.60	20	4	100	7.94 ± 0.36	42.14 ± 0.98	68.84
	0.75	20	4	100	8.31 ± 0.31	40.92 ± 0.73	27.09
	0.90	20	4	100	7.92 ± 0.33	42.61 ± 0.89	21.70
	0.95	20	4	100	7.45 ± 0.37	41.19 ± 0.86	21.51

Table 5: Detailed BOCA results for a reduced number of $Q^{\text{init}} = 20$ initial random queries. We present efficiency loss, relative revenue and runtime of MLCA with our MVNN-based uUB $\mathcal{M}_i^{\text{uUB}}$ as \mathcal{A}_i . Shown are averages including a 95%-normal-CI on a test set of 50 instances in all three considered SATS domains. The best MVNN-based uUBs per domain (w.r.t the quantile parameter q) based on the lowest efficiency loss are marked in grey.

DOMAIN	QUANTILE PARAMETER Q	Q^{INIT}	Q^{ROUND}	Q^{MAX}	EFFICIENCY LOSS IN % \downarrow	REVENUE IN % \uparrow	RUNTIME IN HOURS
LSVM	0.60	20	4	100	0.71 ± 0.43	73.73 ± 3.57	4.87
	0.75	20	4	100	0.71 ± 0.45	74.71 ± 3.32	5.11
	0.90	20	4	100	0.58 ± 0.38	74.81 ± 3.51	12.76
	0.95	20	4	100	0.59 ± 0.34	73.88 ± 3.64	14.11
SRVM	0.60	20	4	100	0.18 ± 0.04	54.13 ± 1.45	30.47
	0.75	20	4	100	0.16 ± 0.04	54.32 ± 1.49	28.62
	0.90	20	4	100	0.29 ± 0.06	54.55 ± 1.51	31.74
	0.95	20	4	100	0.30 ± 0.05	54.35 ± 1.58	30.39
MRVM	0.60	20	4	100	7.73 ± 0.43	42.51 ± 0.75	25.39
	0.75	20	4	100	8.14 ± 0.40	41.46 ± 0.85	7.70
	0.90	20	4	100	7.73 ± 0.41	41.42 ± 0.85	10.06
	0.95	20	4	100	7.52 ± 0.36	41.33 ± 1.11	9.44

Table 6: Detailed OUR-MVNN-MLCA results for a reduced number of $Q^{\text{init}} = 20$ initial random queries. We present efficiency loss, relative revenue and runtime of OUR-MVNN-MLCA, i.e., MLCA with our MVNN-based mean $\mathcal{M}_i^{\text{mean}}$ as \mathcal{A}_i . Shown are averages including a 95%-normal-CI on a test set of 50 instances in all three considered SATS domains.

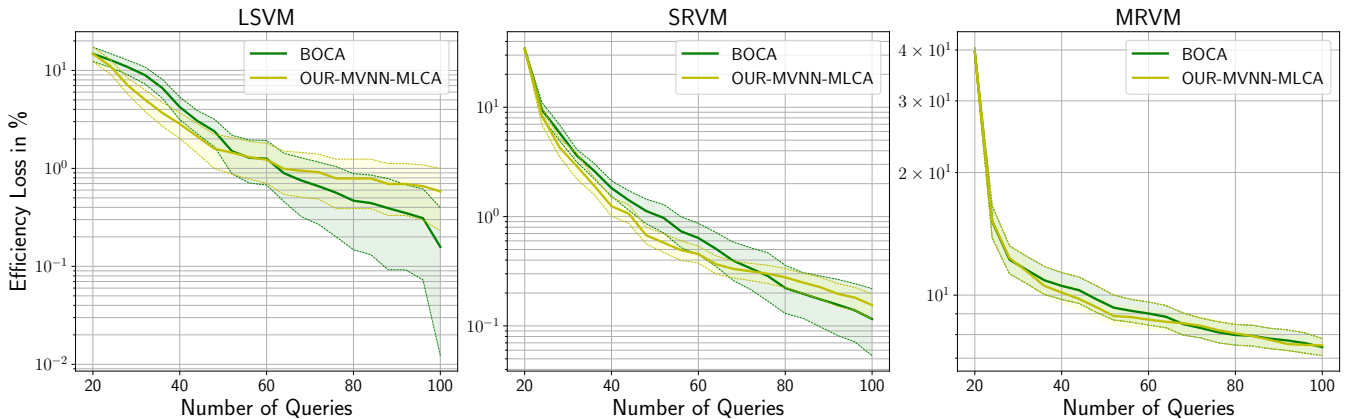


Figure 9: Efficiency loss paths (i.e., regret plots) for a reduced number of initial queries $Q^{\text{init}} = 20$ of BOCA winners (green) from Table 5 compared to OUR-MVNN-MLCA winners (yellow) from Table 6. Shown are averages with 95% CIs over 50 instances.